Astron. Astrophys. 233, 437–455 (1990)

ASTRONOMY AND ASTROPHYSICS

# Decomposition of the FIR Milky Way observed by IRAS

**J.B.G.M. Bloemen**[1,2], **E.R. Deul**[1], **and P. Thaddeus**[3]

[1] Leiden Observatory, P.O. Box 9513, NL-2300 RA Leiden, The Netherlands
[2] Laboratory for Space Research Leiden, P.O. Box 9504, NL-2300 RA Leiden, The Netherlands
[3] Harvard-Smithsonian Center for Astrophysics, 60 Garden Street, Cambridge, MA 02138, USA

Received August 26, 1988; accepted July 25, 1989

**Abstract.** IRAS observations of dust emitting in the 60-μm and 100-μm far-infrared (FIR) bands are compared with H I and CO surveys covering the entire Milky Way. A multivariate correlation analysis is used to decompose the 60-μm and 100-μm maps into components associated with the atomic and molecular gas and to disentangle the line-of-sight integration effects. The velocity information inherent in the H I and CO spectral lines is used as a distance indicator. Regions for which the FIR emission is dominated by warm dust, associated with H II regions, are excluded on the basis of their 60 μm/100 μm colours.

Most of the FIR luminosity of the Galactic disk in the 60-μm and 100-μm bands at $R > 2$ kpc appears to originate from dust associated with neutral atomic gas ($\sim 8$–$11\ 10^9\ L_\odot$) and molecular gas ($\sim 2.5\ 10^9\ L_\odot$) heated by the general interstellar radiation field. Infrared emission from dust associated with H II regions contributes only a minor fraction. Most ($\sim 3/4$) of the Galactic FIR emission originates inside the solar circle: $\sim 6$–$8\ 10^9\ L_\odot$ ($R = 2$–$10$ kpc) from dust associated with H I and essentially all the emission from dust associated with molecular gas.

The FIR dust emissivity per nucleon is found to decrease strongly with increasing Galactocentric distance. This radial emissivity distribution is best determined for dust associated with atomic gas, but there is no indication that the shape of the emissivity distribution for dust mixed with molecular gas is significantly different. In addition, there is no evidence for a large-scale variation of the 60 μm/100 μm emissivity ratio with Galactocentric radius; the average Galactic value is $0.27 \pm 0.03$ for dust mixed with atomic gas and $0.20 \pm 0.06$ for dust in molecular clouds. The strong FIR emissivity gradient suggests a radial decrease in either the intensity of the Galactic interstellar radiation field (estimated to be of the same magnitude) or the dust-to-gas ratio. The former is expected to be the dominant effect, but the absence of an accompanying change in the 60 μm/100 μm ratio is hard to reconcile with the Mathis, Rumpl and Nordsieck, 1977 dust model. The constancy of this ratio confirms previous suggestions that the 60-μm band has a considerable contribution from grains not in thermal equilibrium, such as very small particles briefly heated by the absorption of a single stellar photon.

The ratio between $H_2$ column density and integrated CO line intensity is calibrated simultaneously. A conservative lower limit on the average Galactic value is obtained, $N_{H_2}/W_{CO} > 0.8\ 10^{20}$ molecules cm$^{-2}$ (K km s$^{-1}$)$^{-1}$, but the true average value may well be a factor of 2 or more larger.

*Send offprint requests to:* J.B.G.M. Bloemen

**Key words:** Galactic disk – infrared emission – interstellar dust – IRAS – molecular clouds

## 1. Introduction

The origin of the Galactic FIR emission ($\lambda \approx 30$–$300$ μm) has been the subject of numerous studies in the past decade, largely on the basis of observations obtained with balloon-borne instruments (e.g., Nishimura et al., 1980; Boissé et al., 1981; Gispert et al., 1982; Caux et al., 1984; Hauser et al., 1984; and references therein to pioneering previous missions). It is clear from the modelling performed by these authors, and others (Ryter and Puget, 1977; Mezger et al., 1982; Mathis et al., 1983; Puget, 1985; Cox et al., 1986), that the Galactic FIR emission originates largely from interstellar dust heated by stellar radiation, but several aspects of the models have evolved considerably. In particular, the relative importance of potential heating sources and the relative contributions of dust associated with different phases of the interstellar medium (ISM) to the Galactic infrared emission have been subjects of debate. The availability of the IRAS survey has provided important new insight (see review article by Cox and Mezger, 1989), but unravelling the FIR Milky Way remains complex.

The FIR cirrus observed by IRAS at high Galactic latitudes (Low et al., 1984) correlates well with the column-density distribution of neutral atomic hydrogen (Boulanger et al., 1985; Deul and Burton, 1989; Boulanger and Pérault, 1988). High-latitude molecular clouds, traced by CO observations, are also associated with distinct cirrus features, and for those (parts of) local clouds and cloud complexes that are relatively quiescent – no signs of massive star formation – the CO intensity distribution correlates with the 100-μm intensity distribution (Weiland et al., 1986; de Vries et al., 1987; Heithausen and Mebold, 1988; Boulanger et al., 1989). These findings lead to the conclusion that the interstellar radiation field and the dust properties in the solar vicinity are relatively uniform on scales of the order of 100 pc (Boulanger and Pérault, 1988). Regions of massive star formation – H II regions and their interfaces with molecular clouds – are found, however, to be excessive FIR emitters. The reason is that an OB association is a powerful heating source, that during the initial 30–40% of its lifetime heats mainly the dust in its immediate surroundings (Leisawitz and Hauser, 1988). Although H II regions are intense FIR sources, they appear to contribute only a minor fraction to the total FIR emission from the solar neighbourhood (Boulanger and Pérault, 1988).

Near the Galactic plane ($|b| \lesssim 10°$), the relationship of the observed infrared emission to the different phases of the ISM is much more difficult to determine. Because of the long lines of sight through the Galactic disk, the components are heavily blended and large-scale variations in the infrared emissivity may be important, owing to changes in the dust-to-gas ratio, in the grain properties, and in the intensity of the interstellar radiation field. In addition, correlation studies are hampered by uncertainties in the molecular hydrogen column densities, because the conversion from the observed CO intensities (the best large-scale tracer of the molecular gas) to $H_2$ column densities is still imperfectly understood.

Analyses of the diffuse Galactic $\gamma$-ray emission have encountered similar difficulties. To overcome them, Bloemen et al. (1986) developed a method, based on the maximum-likelihood technique, to disentangle the line-of-sight integration effects and to discern the $\gamma$-ray emission associated with different gas components. This method was applied successfully in correlation studies of the COS-B $\gamma$-ray observations with H I and CO surveys (Bloemen et al., 1986; Strong et al., 1988). In the present paper, a similar method is applied in a comparison between the IRAS surveys (60-µm and 100-µm bands) and H I and CO surveys, because it offers a variety of possibilities: determining the Galactocentric distribution of the FIR emissivity, studying the FIR properties of the dust emission from different gas components separately (particularly atomic and molecular gas), and setting a constraint on the CO-to-$H_2$ conversion factor. Such a complete approach was not feasible in the analyses of previous infrared surveys, because the detection of the extended low-brightness tail of the Galactic-disk emission to higher latitudes was problematic. Accurate mapping of the infrared intensity distribution up to at least 5°–10° from the Galactic plane – achieved with IRAS – is of essential importance for the decomposition into infrared components associated with the different gas phases.

The classical methods of analysis used for previous infrared surveys have recently been applied in several large-scale IRAS studies as well (Deul and Burton, 1989; Broadbent et al., 1989; Pérault et al., 1989; Sodroski et al., 1989). The approaches of Pérault et al. and Sodroski et al. have important similarities to ours. The method of Pérault et al. can be considered as a simplified version of ours, not including the small-scale structure in the data. On the other hand, Sodroski et al. used the small-scale structure but did not account accurately for large-scale infrared emissivity variations throughout the Galaxy. We take into account all the observed structures in the H I, CO, and IRAS maps and allow for large-scale spatial variations in the infrared emissivity as well. Section 2 describes our method and the data used. Estimates of the parameter values in our model and tests of different model versions are presented in Sect. 3. In Sect. 4, the findings are discussed in greater detail and compared with results obtained by others. The conclusions are summarized in Sect. 5.

## 2. Method and data

### 2.1. The model

The work described in this paper consists mainly of a detailed quantitative comparison of the IRAS surveys with H I and CO sky maps for selected Galactocentric distance intervals (the bins are typically a few kpc wide). The H I and CO line velocities were used as distance indicators; on the assumption of circular motions, the line velocity $v$ in the local standard of rest is related to the Galactocentric distance $R$ by $v = (\omega - \omega_0) R_\odot \sin l$, where $\omega = \Theta / R$ and $\Theta(R)$ is the rotation curve of the Galaxy. For the inner Galaxy ($R < R_\odot$)[1] we used the rotation curve of Burton and Gordon (1978) and for the outer Galaxy that of Blitz et al. (1980), as modified by Kulkarni et al. (1982) [i.e., weakly rising up to $R \simeq 18$ kpc, and constant at larger radii]. The radial intervals of $R$ = 2–4, 4–8, 8–10, 10–12, 12–15, and >15 kpc were chosen. These wide intervals are dictated by the requirement that the gas distributions in the rings be distinctly different in order to be able to determine the contribution of each ring to the observed infrared emission (see Sect. 2.2).

We assume that the infrared sky maps for the 60-µm and 100-µm IRAS passbands can be represented as a linear combination of the H I and CO maps of the selected radial intervals – excluding regions with a strong contribution from H II regions, as discussed below. The axial symmetry inherent in this approach allows for only a possible radial dependence of the infrared emissivity. The six radial bins chosen set the resolution of the derived emissivity distribution. The infrared intensity maps for both passbands were fitted to the function

$$I_\lambda = \left( \sum_{i=1}^{6} \varepsilon_\lambda(R_i) \, (N_{\mathrm{H\,I},i} + 2\, Y_\lambda \, W_{\mathrm{CO},i}) \right) + I_{\mathrm{b},\lambda}, \quad [\mathrm{MJy\,sr^{-1}}] \qquad (1)$$

where $\varepsilon_\lambda(R_i)$ $(i = 1, \ldots, 6)$, $Y_\lambda$, and $I_{\mathrm{b},\lambda}$ are free parameters. The parameter $\varepsilon_\lambda(R_i)$ is the infrared emissivity [MJy sr$^{-1}$ (H atom cm$^{-2}$)$^{-1}$] of the dust mixed with the atomic gas in the $i^{\mathrm{th}}$ distance interval, $N_{\mathrm{H\,I},i}$ and $W_{\mathrm{CO},i}$ are the maps of the H I column density and the velocity-integrated CO brightness temperature for this interval, and $I_{\mathrm{b},\lambda}$ is an isotropic infrared background. The parameter $Y_\lambda$ [molecules cm$^{-2}$ (K km s$^{-1}$)$^{-1}$] is the product of the conversion factor $X$ between $W_{\mathrm{CO}}$ and $H_2$ column density ($X \equiv N_{\mathrm{H_2}}/W_{\mathrm{CO}}$) and the ratio of the infrared emissivity of the dust associated with the molecular gas to that of the atomic gas, $\varepsilon_{\lambda,\mathrm{H_2}}/\varepsilon_{\lambda,\mathrm{H\,I}}$. Thus

$$Y_\lambda = \frac{\varepsilon_{\lambda,\mathrm{H_2}}}{\varepsilon_{\lambda,\mathrm{H\,I}}} \cdot X, \qquad (2)$$

where $\varepsilon_{\lambda,\mathrm{H\,I}} \equiv \varepsilon_\lambda$. This parameter $Y_\lambda$ includes effects related to different conditions in the atomic and molecular gas, such as different dust temperatures, dust-to-gas ratios, and dust properties. In Eq. 1, the use of only one $Y_\lambda$ parameter for each passband implies that $X$ and $\varepsilon_{\lambda,\mathrm{H_2}}/\varepsilon_{\lambda,\mathrm{H\,I}}$ (or more precisely, their product) are constrained to be independent of Galactocentric radius. To test whether this assumption is reasonable, we considered a model with two $Y_\lambda$ parameters for each passband, one for $R < 8$ kpc (i.e., the inner two rings), the other for $R > 8$ kpc (the outer four rings). Ideally, a $Y_\lambda$ parameter would be introduced for each ring, but this seems to lead to an over-interpretation of the data.

The infrared emission from warm dust associated with ionized gas in low-density H II regions, heated by OB stars (Drapatz, 1979;

[1] We adopted $R_\odot = 10$ kpc. Using the value $R_\odot = 8.5$ kpc recommended by the IAU, with another standard rotation curve, has only a small effect on the parameters determined in this paper and does not affect the general conclusions. To first order, however, the luminosity estimates obtained in Sect. 4.4 are decreased by a factor of $\sim(8.5/10)^2 \simeq 0.72$.

Mezger, 1978), is not included in our model, simply because this is very hard to accomplish. Fortunately, model estimates of this contribution to the infrared luminosity of the Galactic disk have decreased considerably from about 60–80% (Mezger et al., 1982; Cox et al., 1986) to about only 20% in recent work (Cox and Mezger, 1988). Further, as noted above, Boulanger and Pérault (1988) found that at least in the solar vicinity most of the infrared emission comes from interstellar matter not associated with OB star formation. Our findings indicate that FIR emission from warm dust mixed with ionized gas indeed contributes only a minor fraction to the total Galactic luminosity. Nevertheless, warm dust heated by local sources of radiation may contribute significantly to the infrared intensity in several regions near the Galactic plane. We partly eliminated the contaminating contribution of such H II regions by excluding from the fit those bins with 60 μm/100 μm intensity ratios exceeding 0.35 (corresponding to dust temperatures $T_d \gtrsim 27$ K, for a $\lambda^{-2}$ emissivity law). All excluded bins coincide with the positions of known H II regions. Owing to the line-of-sight integration of cold and warm dust, this criterion rejects only regions most affected by the presence of H II, but we verified that our results do not depend sensitively on the actual criterion used (Sect. 3.3).

Although our modelling is a significant improvement compared with other recent large-scale analyses of the IRAS observations (discussed in the Introduction), it is still a fairly gross approximation of the real Galaxy. One clear over-simplification is the assumption of axial symmetry in the emissivity distribution. This assumption implies that, throughout a certain ring, the dust infrared emissivity per unit of mass for the H I and $H_2$ gas components is constant, although different for these two components via the $Y_\lambda$ parameter. In more physical terms, parameters such as the dust-to-gas ratio and the dust temperature in each gas component are taken to be constant throughout the ring. The assumption of a constant dust temperature is evidently not justified if local heating sources, like OB stars, play an important role. It seems, however, as shown below, that by excluding regions with 60 μm/100 μm intensity ratios >0.35, we have largely eliminated this difficulty.

The region fitted was limited to the latitude range $|b| < 10°$ owing to the poor sky coverage of the CO observations at higher latitudes. Further, including high-latitude regions would give the 8–10 kpc and 10–12 kpc rings excessively high weights in the fit, and as a result any systematic error at high latitudes would strongly bias the solution. We also excluded two 20° wide longitude intervals, centered on the Galactic center and anticenter directions, because of the poor kinematic distance information there.

### 2.2. Data

We used the infrared sky maps derived from the Zodiacal Observations History File (see IRAS Explanatory Supplement, 1985), corrected for contamination by zodiacal emission as modelled by Deul and Wolstencroft (1988). Maps of the 60-μm and 100-μm emission are shown in Fig. 1 a, b; the excluded bins contaminated by H II regions are indicated in Fig. 1 c. We restricted the analysis to the 60-μm and 100-μm bands because of a probably strong contribution from circumstellar (rather than truly interstellar) dust to the emission in the 12-μm and 25-μm IRAS bands. In addition, the uncertainties in the zodiacal contribution at 12 μm and 25 μm are substantial.

The 21-cm H I line surveys of Weaver and Williams (1973; $10° \lesssim l \lesssim 250°$) and Kerr et al. (1986; $240° \lesssim l \lesssim 350°$) were used to derive H I column densities ($|b| \lesssim 10°$). The data were first calibrated to the brightness temperature scale of Williams (1973) and then column densities were derived, correcting for optical depth effects on the assumption of a uniform spin temperature of 125 K. Figure 2 shows the H I column-density maps for the selected radial distance intervals. For completeness the maps include some data from surveys not used in the correlation analysis, in particular part of the survey by Strong et al. (1982; $350° \lesssim l \lesssim 10°$) and the surveys at $|b| \gtrsim 10°$ by Heiles and Habing (1974) and Heiles and Cleary (1979).

The CO ($J = 1 \rightarrow 0$) data used are a composite of several surveys carried out with the Columbia 1.2-m telescope in New York City and on Cerro Tololo in Chile and includes essentially all the data in the large-scale panorama published by Dame et al. (1987). It covers the entire Galactic disk up to $|b| \simeq 7°$, with several large extensions to higher latitudes. Figure 3 presents maps of the integrated CO brightness temperature for the selected rings. The two outer rings have been combined ($R > 12$ kpc), because there is little of CO in the far outer Galaxy.

For intercomparison, the infrared, H I, and CO maps should have approximately the same angular resolution. The CO observations have the lowest (0°.5), and we therefore smoothed the infrared and H I maps to the same resolution as that of the CO data. This procedure is relatively simple, because the CO observations were obtained using a "superbeam" scanning technique over 0°.5 × 0°.5, which we simulated by averaging the infrared and H I data over 0°.5 × 0°.5 bins.

In order to be able to estimate the parameter values in our model, the angular distribution of the gas should vary significantly from distance interval to interval. This must also be the case for the H I and CO maps of the individual intervals in order to determine the $Y_\lambda$ parameter. The six intervals are chosen to satisfy these conditions: as Figs. 2 and 3 indicate, the distributions reveal distinct differences. The degree of similarity among the distributions is reflected in the formal uncertainties resulting from the fitting procedure.

### 2.3. The fitting procedure

A maximum-likelihood analysis, similar to that applied by Bloemen et al. (1986) to the COS-B $\gamma$-ray observations, was used to determine the values of the parameters $\varepsilon_\lambda(R_i)$ $(i = 1, \ldots, 6)$, $Y_\lambda$, and $I_{b,\lambda}$ for the 60-μm and 100-μm passbands. A detailed description of the likelihood method is given by Kendall and Stuart (1973). The formal uncertainty of each parameter was derived from the distribution of the maximum-likelihood ratio for that parameter, $\Lambda = L/L^*$, defined as the ratio between the likelihood, $L$, maximized over the remaining parameters and the maximum likelihood, $L^*$, i.e., the likelihood maximized over all parameters (see, e.g., Eadie et al., 1971). The quantity $-2 \ln \Lambda$ has in this case a $\chi^2$ distribution with one degree of freedom. Similarly, the likelihood ratio was used to compare different versions of the model (i.e., with differing numbers of free parameters; see Sect. 3); for two different model versions, say A and B, $\Lambda = L^A/L^B$. If $\Delta N$ is defined as the number of free parameters of one version relative to another, then $-2 \ln \Lambda$ is distributed as $\chi^2_{\Delta N}$. The corresponding probability of obtaining a value of $-2 \ln \Lambda$ greater than that derived is defined as $P$ in the following presentation of the results.

To calculate likelihood ratios it is necessary to know the noise distribution of the infrared intensities. We selected several high-latitude regions of relatively uniform intensity and found that the noise can be described typically by Gaussian distributions with rms values of $\sigma_{60} = 0.08$ MJy sr$^{-1}$ and $\sigma_{100} = 0.2$ MJy sr$^{-1}$. In the

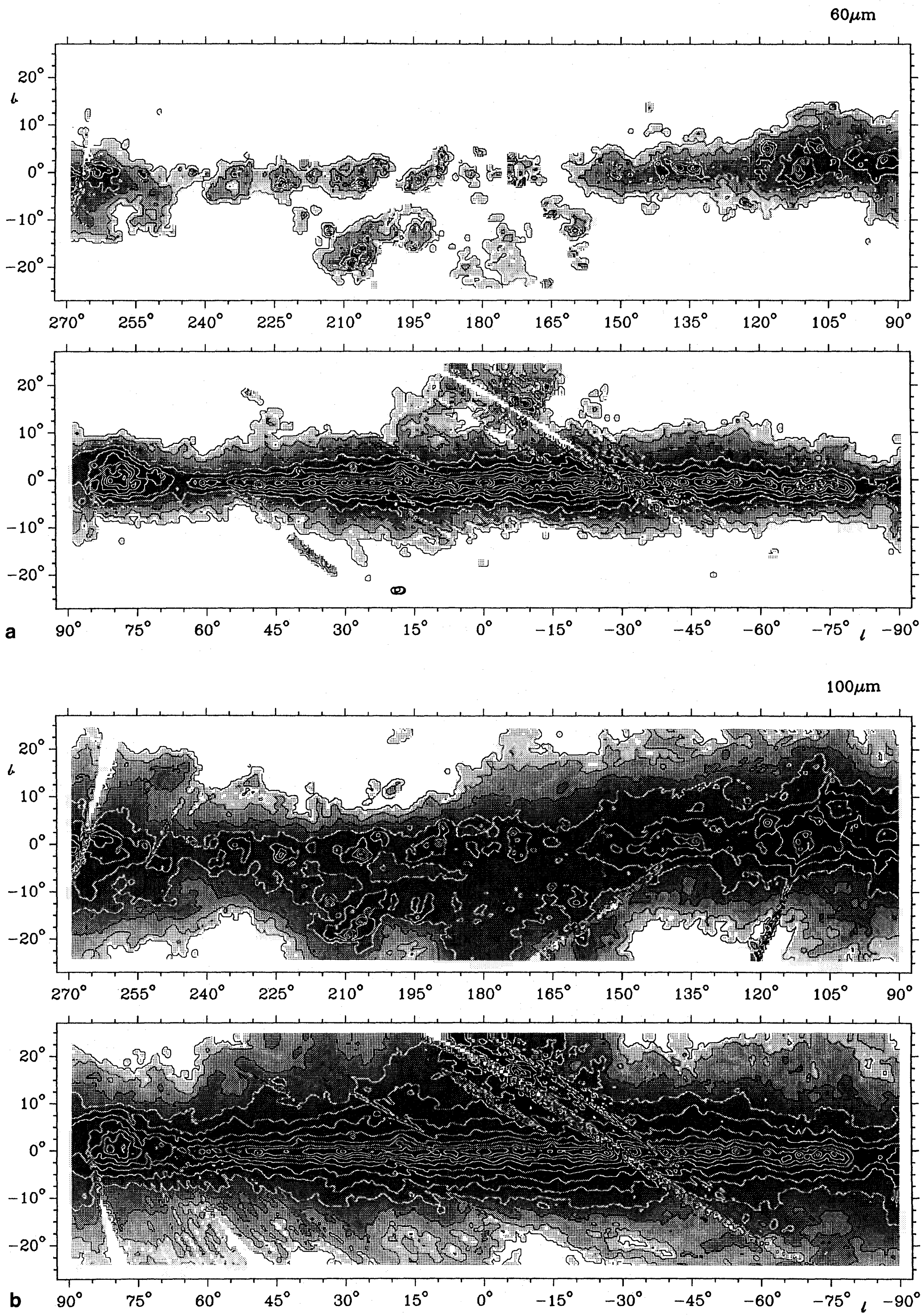


**Fig. 1a–c.** IRAS sky maps of the Milky Way for the 60-μm **a** and 100-μm **b** passbands. The contribution of zodiacal dust has been subtracted using the model of Deul and Wolstencroft (1988). The striping artifacts visible in the maps are due to gain changes between consecutive scans of the satellite, missing scans, or uncertainties in the zodiacal model. Contours at 60 μm: 1.0, 2.0, 4.1, 8.2, 16.4, 33.1, 67, 134, 270, 544, 1096, 2208, and 4447 MJy sr$^{-1}$. Contours at 100 μm: 1.0, 2.1, 4.5, 9.5, 20.1, 42.5, 90, 190, 403, 854, 1808, 3827, and 8103 MJy sr$^{-1}$. Map **c** shows an outline of the region fitted (black) and the positions of the pixels inside this region excluded from the analysis, either because of striping artifacts or because of the presence of intense H II regions (see Sect. 2.1)

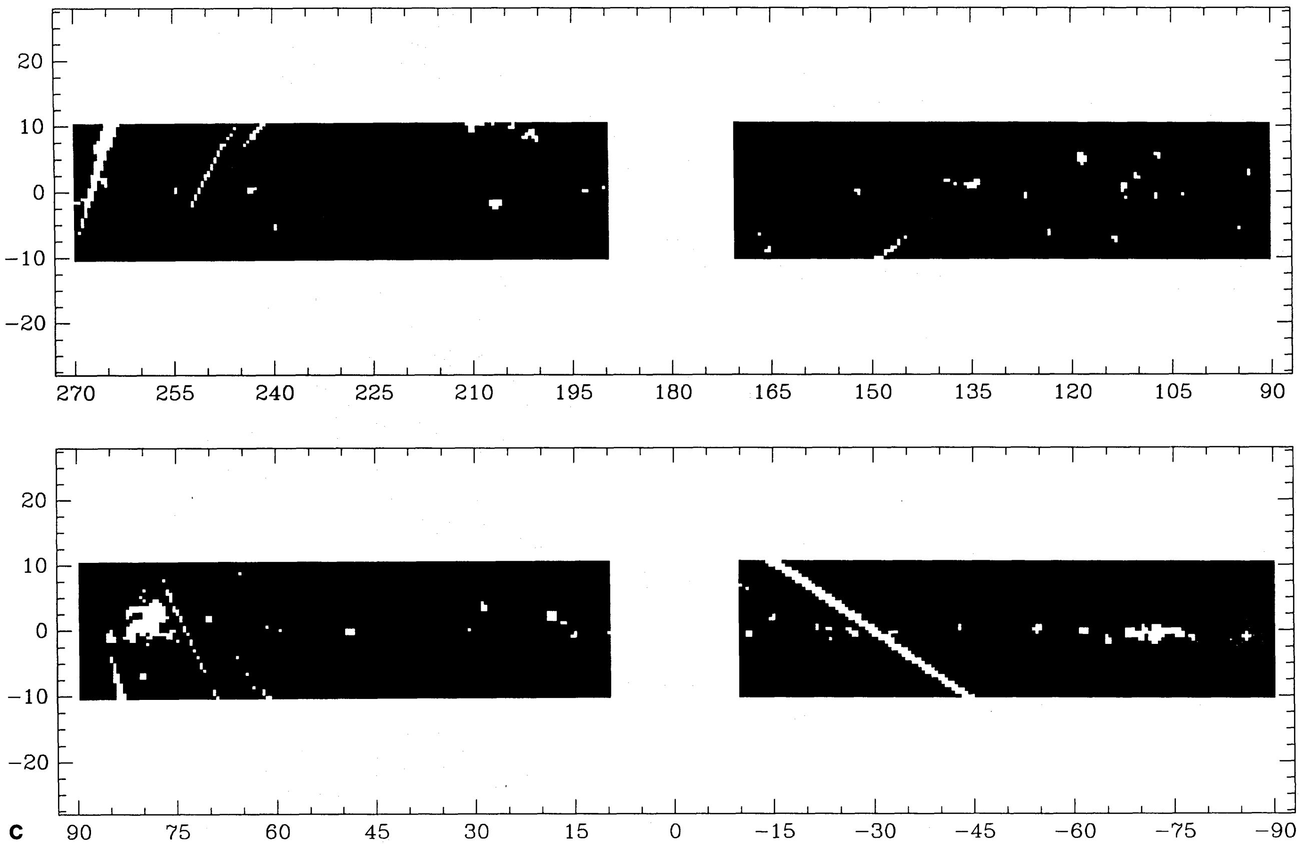


**Fig. 1** (continued)

calculations presented here, these values were used for each pixel. All directions in the region fitted therefore have the same weight. Should one wish to scale the rms values by a factor $f$, then the $-2\ln\Lambda$ values given here should be multiplied by $f^{-2}$; the parameter estimates would not be affected. Owing to possible systematic uncertainties in the data, the resulting likelihood-ratio values should not be adopted uncritically.

Because of the Gaussian shape of the noise distribution, finding the maximum likelihood is equivalent to a least-squares analysis:

$$L^* = \prod \frac{1}{\sigma_\lambda \sqrt{2\pi}} \exp\left(\frac{-(I_\lambda - I_\lambda^*)^2}{2\sigma_\lambda^2}\right), \tag{3}$$

where the product is over all sky pixels in the comparison, $I_\lambda$ is the observed infrared intensity distribution for the two passbands, and $I_\lambda^*$ is the modelled intensity distribution with parameter values such that $L$ is maximized ($L^*$). The likelihood ratio between two model versions A and B is in our analysis given by the expression

$$-2\ln\Lambda = \frac{1}{\sigma_\lambda^2} \sum \left[(I_\lambda - I_\lambda^{\mathrm{A}})^2 - (I_\lambda - I_\lambda^{\mathrm{B}})^2\right], \tag{4}$$

where the summation is over all sky pixels in the comparison, $I_\lambda$ is the observed infrared intensity distribution for the two passbands, and $I_\lambda^{\mathrm{A}}$ and $I_\lambda^{\mathrm{B}}$ are the modelled intensity distributions. The impact of scaling $\sigma_\lambda$, mentioned above, is evident from this expression.

## 3. Results

Table 1 lists various versions of the model fitted to the data and the resulting likelihood ratios relative to the most general version. Each version has different constraints on the fit parameters, discussed below in detail. Table 2 summarizes the hypothesis tests we have made, i.e., comparisons of the relative goodness of fits of the model versions. Table 3 gives the parameter estimates for each version. The reader is referred to these tables throughout the following discussion of the results.

### 3.1. *Test of radial dependence of the infrared emissivity $\varepsilon_\lambda$*

In the most general version of our model (case 4 in Table 1) each of the parameters is free, for a total of $2\times 8=16$. To test the hypothesis that $\varepsilon_\lambda$ is independent of $R$, we performed a fit with $\varepsilon_\lambda(R)=$ constant for both the 60-µm and 100-µm bands (case 0). A comparison of cases 4 and 0 gives $-2\ln\Lambda=69.8$, which with $\Delta N=16-6=10$ corresponds to $P\simeq 10^{-11}$. It is safe therefore to reject the hypothesis of a constant emissivity.

Figure 4, which shows the radial emissivity distributions for the 60-µm and 100-µm bands, indicates a pronounced increase in the emissivity towards the Galactic center. The value for the 2–4 kpc ring is not accurately determined, because the emission from this ring is projected onto a very small region of the sky, much of which we excluded from our analysis because of the poor kinematic distance information whithin 10° from the Galactic center (compare Fig. 1c with Figs. 2 and 3). There is no evidence,

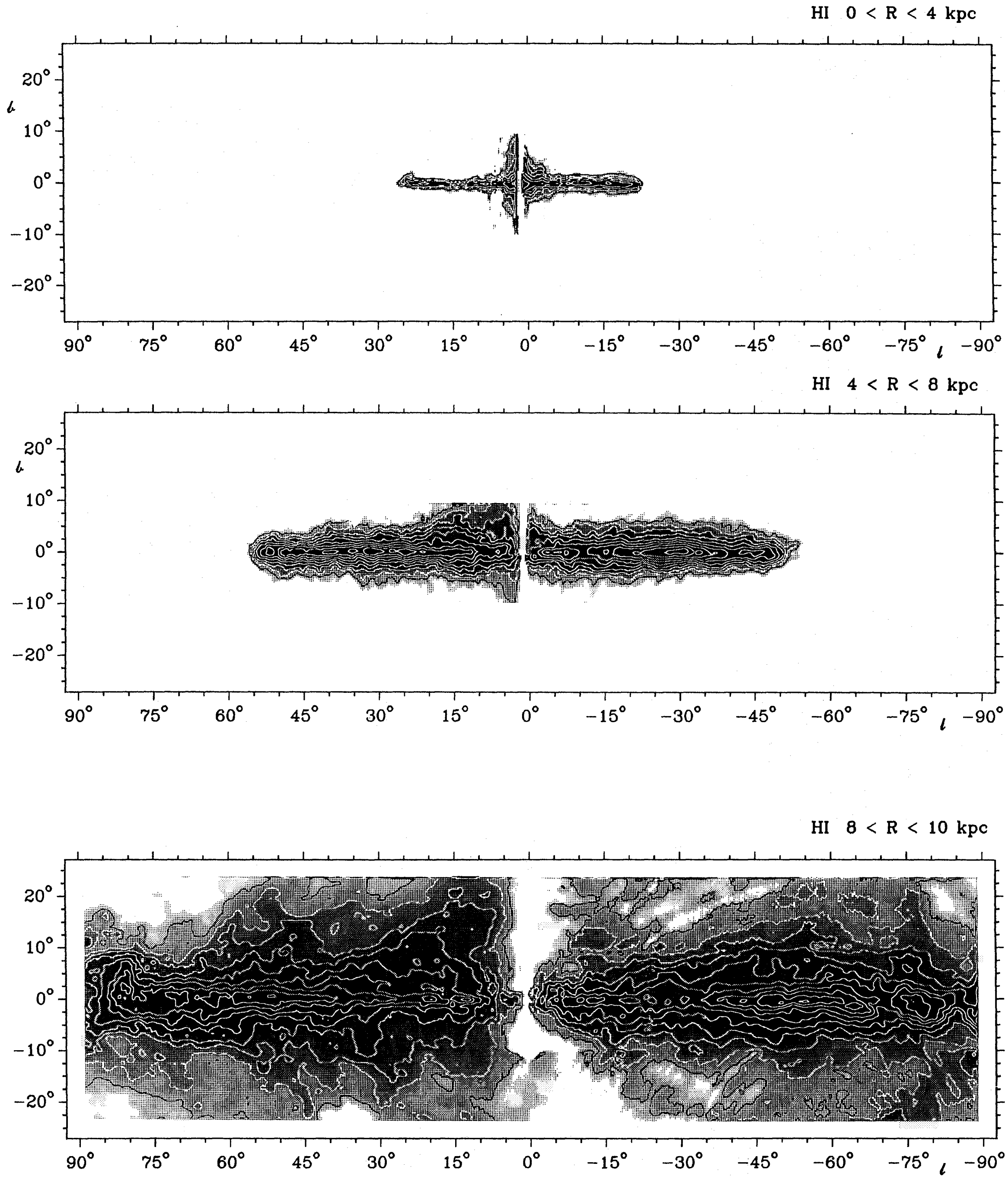


**Fig. 2.** H I column-density maps of the Milky Way for selected Galactocentric distance intervals (indicated at the top). The maps were constructed from a combination of several H I 21-cm surveys, described in Sect. 2. Contours: 5.5, 8.2, 12.2, 18.1, 27, 40.3, 60.2, 90, 134, 200, 298, 445, 663, and 990 $10^{20}$ H atom cm$^{-2}$

however, that the emissivity distribution peaks near the molecular ring at $R \simeq 5$ kpc, nor that it flattens for $R < 5$ kpc.

### 3.2. *Tests of wavelength dependence of $Y_\lambda$ and $\varepsilon_\lambda(R)$*

Case 1 is the most restricted version of the model remaining after we have rejected case 0. In this version, both $Y_\lambda$ and the shape of the radial emissivity distribution are wavelength independent, i.e., $Y_{60} = Y_{100}$ and $\varepsilon_{60}(R)/\varepsilon_{100}(R) = \text{constant}$, with a total of 10 free parameters. Between the most general case (4) and this most restricted one are two intermediate versions in which either $\varepsilon_{60}(R)/\varepsilon_{100}(R) = \text{constant}$ (case 2) or $Y_{60} = Y_{100}$ (case 3). The likelihood values of all four cases were used to test the following null hypotheses ($H_0$), consisting of constraints on the wavelength dependence of either $Y_\lambda$ or $\varepsilon_\lambda(R)$, against the alternative hypothesis that the constraint does not apply. Following common practice, we can set a *level of significance* for our tests at 1%, but owing to possible systematic uncertainties, we should not blindly accept the resulting probability values.

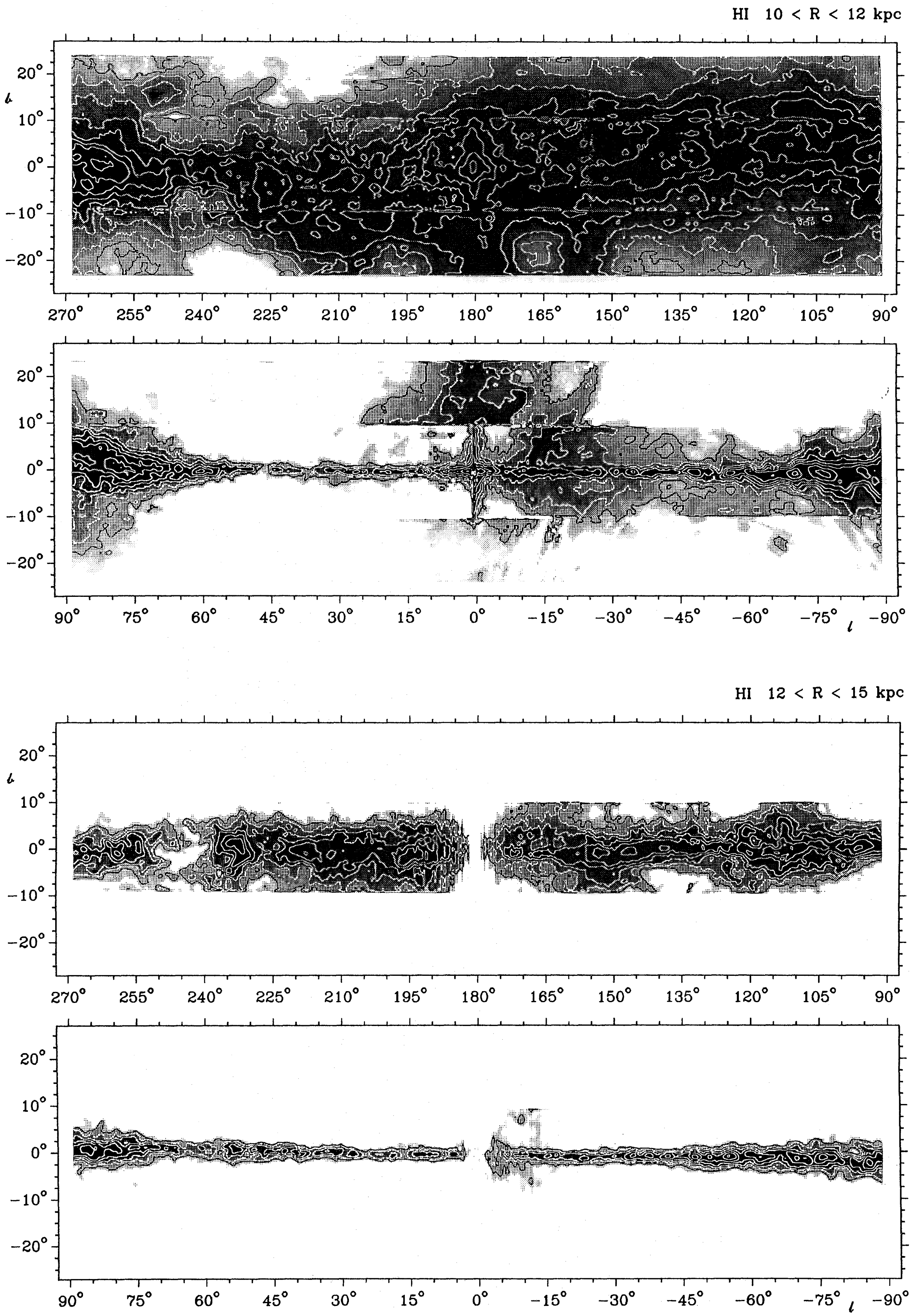


**Fig. 2** (continued)

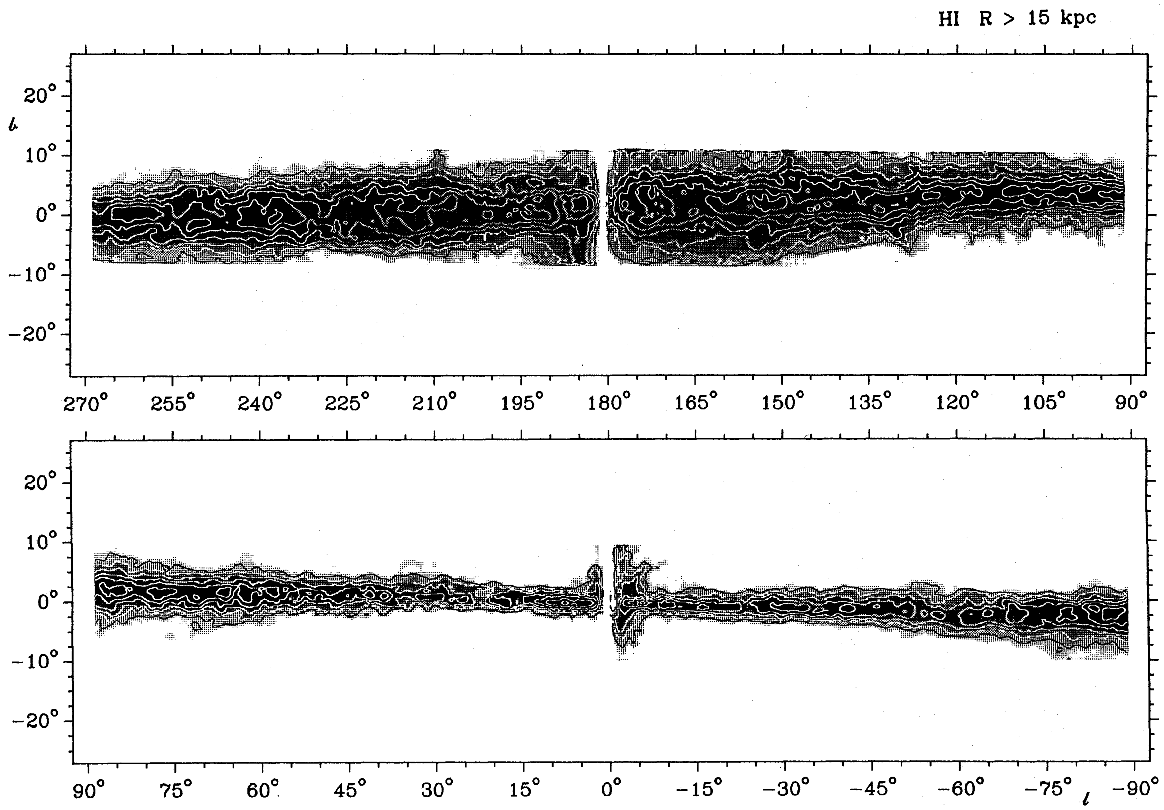


**Fig. 2** (continued)

(a) $H_0$: $\varepsilon_{60}(R)/\varepsilon_{100}(R) = \text{constant}$

This hypothesis can be tested in two ways. A comparison of cases 4 and 2 gives $-2\ln\Lambda = 1.5$, $\Delta N = 5$, and $P = 0.9$. A comparison of cases 3 and 1 amounts to setting constraints on the parameter family of case 3, in which $Y_\lambda$ is already constrained to $Y_{60} = Y_{100}$. This gives $-2\ln\Lambda = 14.4$, $\Delta N = 5$, and $P = 0.01$. Neither test rejects $H_0$, although the outcome of the second test is just at the chosen level of significance. If we do not reject $H_0$ we make no decision, and thus no error. We conclude that no significant evidence exists for a difference in the radial distributions of the infrared emissivity at 60 µm and 100 µm.

(b) $H_0$: $Y_{60} = Y_{100}$

This hypothesis, as Eq. 2 makes clear, is equivalent to $\varepsilon_{60,\mathrm{H_2}}/\varepsilon_{100,\mathrm{H_2}} = \varepsilon_{60,\mathrm{H\,I}}/\varepsilon_{100,\mathrm{H\,I}}$, i.e., equal 60 µm/100 µm emissivity ratios for the infrared emission associated with atomic and molecular gas. This hypothesis, too, can be tested in two ways. A comparison of cases 4 and 3 gives $-2\ln\Lambda = 3.7$, $\Delta N = 1$, and $P = 0.05$. We therefore cannot reject $H_0$ on the basis of this test. A comparison of cases 2 and 1 amounts to setting constraints on the parameter family of case 2, in which $\varepsilon_\lambda(R)$ is already constrained to $\varepsilon_{60}(R)/\varepsilon_{100}(R) = \text{constant}$. This test gives $-2\ln\Lambda = 16.6$, $\Delta N = 1$, and $P = 5\ 10^{-5}$, and hence decisively rejects $H_0$. The results of these two tests are not mutually inconsistent, because the second probably has more *power*. We conclude that the $Y_{60}$ and $Y_{100}$ values differ. In other words, not surprisingly, we find evidence that the 60 µm/100 µm ratios of the emission from atomic and molecular gas are different.

### *3.3. The preferred model and goodness of fit*

In summary, the tests indicate that

(i) the infrared emissivity per H atom, $\varepsilon_\lambda(R)$, decreases significantly with increasing Galactocentric radius,

(ii) the 60/100 µm emissivity ratio is constant as a function of $R$ within uncertainties, and

(iii) the $Y_\lambda$ parameter is wavelength dependent with $Y_{100} > Y_{60}$ (Table 3), implying that $\varepsilon_{60,\mathrm{H_2}}/\varepsilon_{100,\mathrm{H_2}} < \varepsilon_{60,\mathrm{H\,I}}/\varepsilon_{100,\mathrm{H\,I}}$.

Case 2 is the preferred model. Its fit to the data is not significantly worse than that of the most general version (case 4) and significantly better than that of the most restricted version (case 1). The likelihood value of case 3, however, is almost the same as that of case 2 (Table 1), which indicates that case 3 fits the data almost as well as case 2; the difference in the significance of the wavelength dependences results from the different number of parameters.

In the models considered above, $Y_\lambda$ is assumed to be independent of Galactocentric distance. To verify the correctness of this assumption, an additional free parameter was introduced in case 2, namely $r \equiv Y_\lambda(2\text{–}8\,\mathrm{kpc})/Y_\lambda(>8\,\mathrm{kpc})$, independent of wavelength (case $2r$ in the following). A comparison of case $2r$ with case 2 amounts to testing the hypothesis that $r = 1$. We found $-2\ln\Lambda = 0.3$, which with $\Delta N = 1$ yields $P = 0.6$, so the hypothesis that $r = 1$ cannot be rejected. In other words, we find no evidence for a large-scale radial variation of $Y_\lambda$ and hence case 2 remains the preferred model. We are left with a relatively simple model in which the 60 µm/100 µm ratio of the infrared emissivity (per nucleon) is independent of $R$, but this ratio is smaller for emission from dust associated with molecular gas than for emission from dust associated with atomic gas (see Section 3.4).

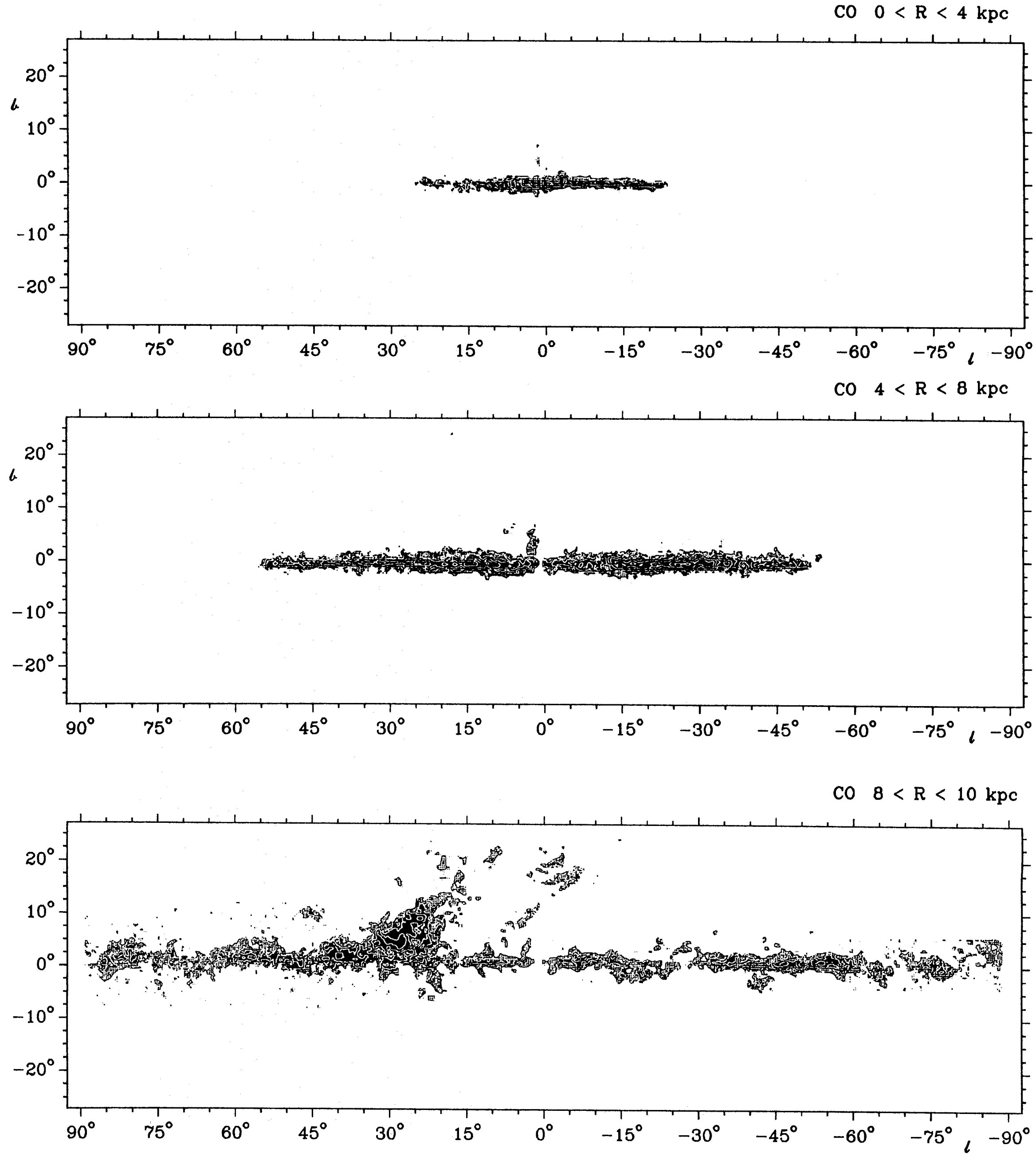


**Fig. 3.** Sky maps of the integrated CO intensity for selected Galactocentric distance intervals (indicated at the top). The database used is a composite of several surveys carried out with the Columbia telescopes, summarized by Dame et al. (1987). Contours: 3.3, 4.9, 7.4, 11.0, 16.4, 30, 37 K km s$^{-1}$

Figures 5 and 6 show longitude profiles of the observed 60-μm and 100-μm intensities and those expected from case 2. Figure 7 shows latitude profiles. The regions excluded from the fit because of the presence of intense H II regions and poor kinematic distance information are not included in these profiles (neither in the observations nor in the model). The figures indicate a generally good agreement between the modelled dust emission based on the H I and CO data and the infrared observations. Particularly at 60 μm, however, some strong peaks in the data are not fitted by the model. These are probably largely the remaining H II regions not excluded by our criterion (Sect. 2.1), which the longitude profiles suggest did not have a strong influence on the fitting process, because most peaks appear to be excesses on top of our model predictions. This finding may not be surprising, because the peaks contribute to only a minor fraction of the total number of pixels fitted. It gives further assurance that the results do not depend sensitively on the criterion for exclusion of H II regions.

### 3.4. *The Galactic 60 μm/100 μm colours*

Our best estimates of the $Y_\lambda$ parameter (from case 2) are $Y_{60} = (0.65 \pm 0.11)\ 10^{20}$ and $Y_{100} = (0.84 \pm 0.20)\ 10^{20}$ molecules cm$^{-2}$ (K km s$^{-1}$)$^{-1}$, which yield

$$\frac{\varepsilon_{60,\mathrm{H_2}}}{\varepsilon_{100,\mathrm{H_2}}} \Big/ \frac{\varepsilon_{60,\mathrm{H\,I}}}{\varepsilon_{100,\mathrm{H\,I}}} \equiv \frac{Y_{60}}{Y_{100}} = 0.8 \pm 0.2. \qquad (5)$$

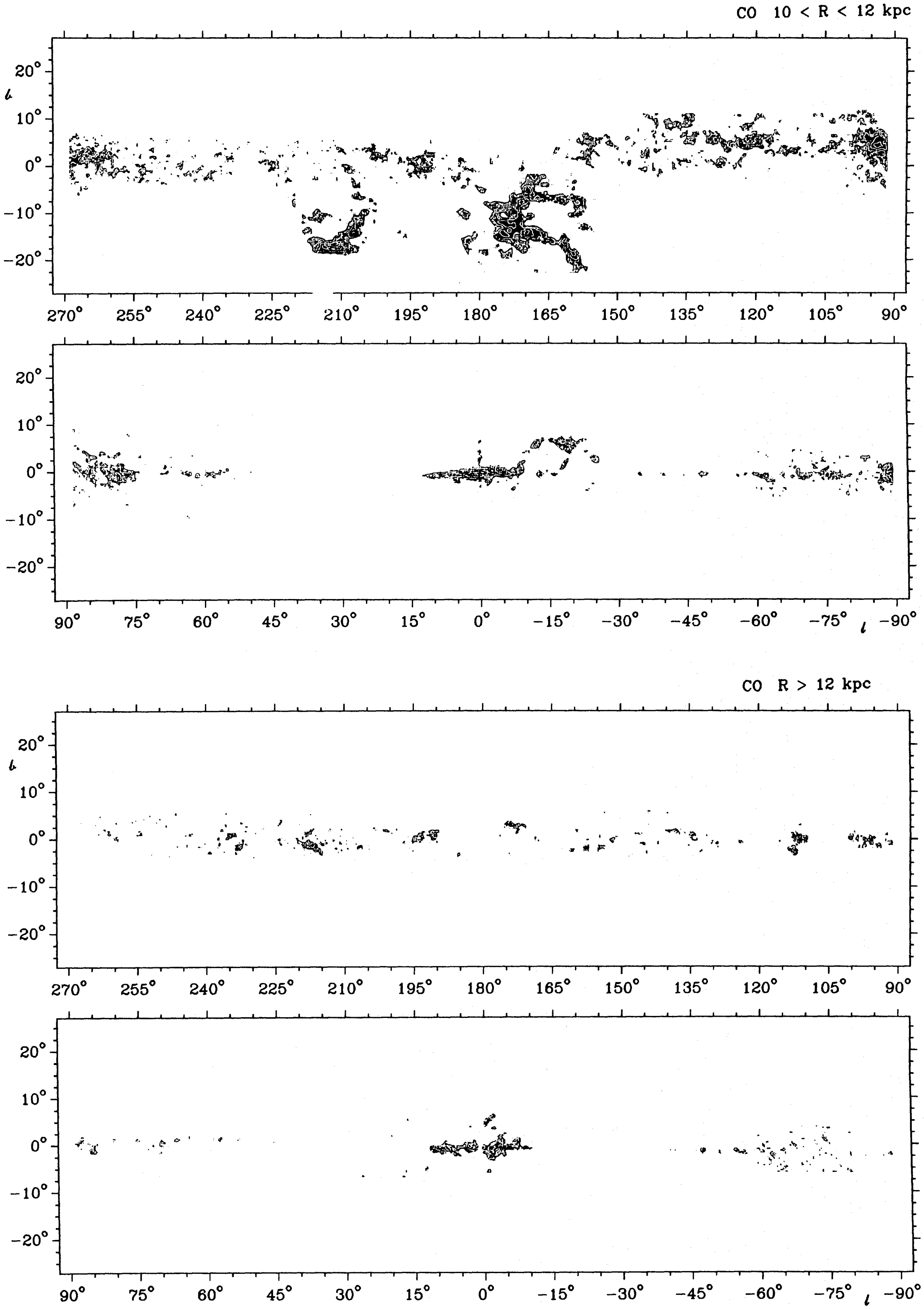


**Fig. 3** (continued)

**Table 1.** Summary of fits

| Case | $\varepsilon_\lambda(R)$ constraints | $Y_\lambda$ constraints | Number of free parameters | $-2\ln\Lambda$ relative to case 4 |
|---|---|---|---|---|
| 0 | $\varepsilon_\lambda(R)=$ const. (60 and 100 µm) | None | 6 | 69.8 |
| 1 | $\varepsilon_{60}(R)/\varepsilon_{100}(R)=$ const. | $Y_{60}=Y_{100}$ | 10 | 18.1 |
| 2 | $\varepsilon_{60}(R)/\varepsilon_{100}(R)=$ const. | None | 11 | 1.5 |
| $2r$ [a] | $\varepsilon_{60}(R)/\varepsilon_{100}(R)=$ const. | None | 12 | 1.2 |
| 3 | None | $Y_{60}=Y_{100}$ | 15 | 3.7 |
| 4 | None | None | 16 | 0 |

[a] A free parameter $r=Y_\lambda(2\text{–}8\,\text{kpc})/Y_\lambda(>8\,\text{kpc})$ is introduced in case $2r$.

**Table 2.** Summary of hypothesis tests

| Null hypothesis | Cases | $-2\ln\Lambda$ | Number of degrees of freedom | $P$ |
|---|---|---|---|---|
| *Tests of radial dependence:* | | | | |
| $\varepsilon_\lambda(R)=$ const. (60 and 100 µm) | 4 vs 0 | 69.8 | $16-6\ =10$ | $\sim 10^{-11}$ |
| $r=1$ | $2r$ vs 2 | 0.3 | $12-11=1$ | 0.6 |
| *Tests of wavelength dependence:* | | | | |
| $Y_{60}=Y_{100}$ | 2 vs 1 | 16.6 | $11-10=1$ | $5\ 10^{-5}$ |
| | 4 vs 3 | 3.7 | $16-15=1$ | 0.05 |
| $\varepsilon_{60}(R)/\varepsilon_{100}(R)=$ const. | 3 vs 1 | 14.4 | $15-10=5$ | 0.01 |
| | 4 vs 2 | 1.5 | $16-11=5$ | 0.9 |

**Table 3.** Parameter estimates

| Parameter | Case 2 | | Case 3 | | Case 4 | |
|---|---|---|---|---|---|---|
| | 60 µm | 100 µm | 60 µm | 100 µm | 60 µm | 100 µm |
| $\varepsilon_\lambda(R_1)$ | 5.4 | 20.0 | 5.0 | 21.4 | $4.7\ \pm 1.3$ | $18.0\ \pm 2.9$ |
| $\varepsilon_\lambda(R_2)$ | 1.1 | 3.9 | 1.1 | 4.2 | $1.0\ \pm 0.3$ | $4.0\ \pm 1.0$ |
| $\varepsilon_\lambda(R_3)$ | 0.35 | 1.3 | 0.39 | 1.5 | $0.51\pm 0.10$ | $1.8\ \pm 0.5$ |
| $\varepsilon_\lambda(R_4)$ | 0.10 | 0.35 | 0.12 | 0.48 | $0.10\pm 0.02$ | $0.39\pm 0.09$ |
| $\varepsilon_\lambda(R_5)$ | 0.13 | 0.48 | 0.13 | 0.54 | $0.12\pm 0.03$ | $0.46\pm 0.11$ |
| $\varepsilon_\lambda(R_6)$ | 0.08 | 0.28 | 0.07 | 0.26 | $0.08\pm 0.02$ | $0.30\pm 0.07$ |
| $Y_\lambda$ | 0.65 | 0.84 | 0.71 | | $0.58\pm 0.11$ | $0.76\pm 0.20$ |
| $I_{b,\lambda}$ | 0.39 | 2.0 | 0.40 | 2.0 | $0.39\pm 0.08$ | $2.1\ \pm 0.3$ |

$R_1$ *to* $R_6$ correspond to $R=2$–4, 4–8, 8–10, 10–12, 12–15, and $>15$ kpc.

*Units:*

$\varepsilon_\lambda(R_i)$: MJy sr$^{-1}$ ($10^{20}$ H atom cm$^{-2}$)$^{-1}$
[for comparison, this unit corresponds to $4\pi\lambda\varepsilon_\lambda$ values of $6.28\ 10^{-31}$ W (H atom)$^{-1}$ or 1.92 $L_\odot/M_\odot$ in the 60-µm band and $3.77\ 10^{-31}$ W (H atom)$^{-1}$ or 1.15 $L_\odot/M_\odot$ in the 100-µm band]

$Y_\lambda$: $10^{20}$ molecules cm$^{-2}$ (K km s$^{-1}$)$^{-1}$

$I_{b,\lambda}$: MJy sr$^{-1}$

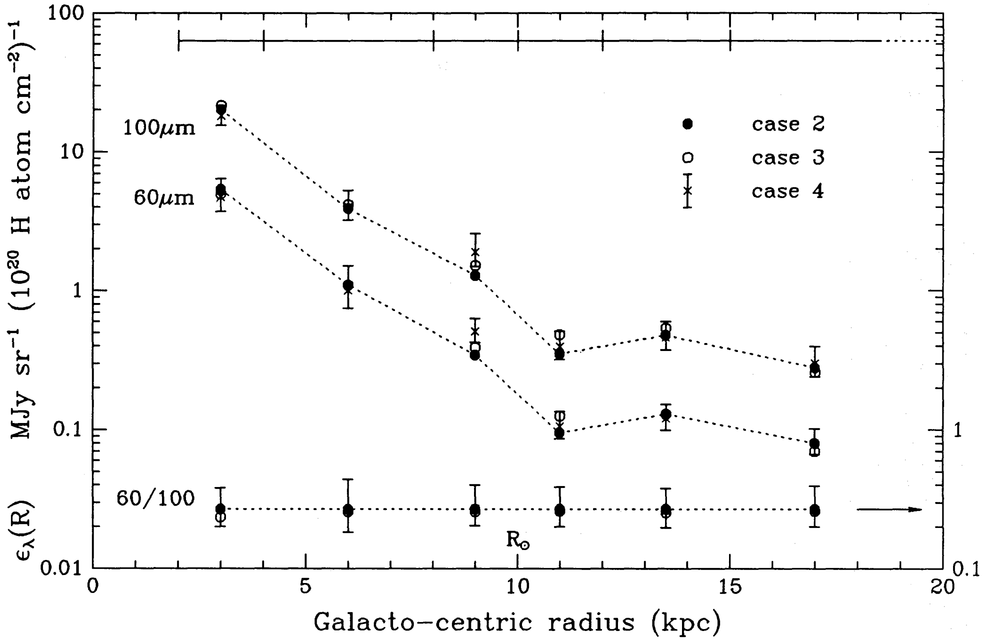


**Fig. 4.** Galactocentric distributions of the infrared emissivity of dust associated with atomic gas for the 60-μm and 100-μm bands; the shapes are similar with a 60 μm/100 μm ratio of $0.27 \pm 0.03$. Within the uncertainties of the analysis, the radial dependence of the emissivity distribution for dust associated with molecular gas does not differ from that for the atomic gas, but the 60 μm/100 μm emissivity ratio is $0.20 \pm 0.06$

With the ratio of the radial emissivity distributions of dust associated with the atomic component of the interstellar gas,

$$\frac{\varepsilon_{60,\,\mathrm{H\,I}}}{\varepsilon_{100,\,\mathrm{H\,I}}} = 0.27 \pm 0.03, \qquad (6)$$

Equation 5 yields for the corresponding ratio of dust associated with the molecular component

$$\frac{\varepsilon_{60,\,\mathrm{H_2}}}{\varepsilon_{100,\,\mathrm{H_2}}} = 0.20 \pm 0.06. \qquad (7)$$

These values can be considered global Galactic averages (beyond $R \simeq 3$ kpc), because we found no significant evidence for variations as a function of $R$ on scales of a few kpc. For a $\lambda^{-2}$ emissivity law, the 60 μm/100 μm ratios given by Eqs. 6 and 7 correspond to dust temperatures of about 24 K for dust mixed with the atomic gas and about 22 K for that mixed with the molecular gas. These temperatures are, of course, unreliable if the dust particles are not in thermal equilibrium – see Sect. 4.2.

## 4. Discussion

### 4.1. Comparison with local FIR properties at high latitudes

Before discussing the results of our analysis in further detail, we briefly compare our parameter estimates near $R_\odot$ and those obtained from analyses of local regions at high latitudes.

Several studies of the relation between the 100-μm intensity and the H I column density for selected high-latitude regions have been reviewed by Beichman (1987), who, averaging the various determinations of the 100-μm emissivity, found $\varepsilon_{100,\,\mathrm{H\,I}} = 1.0 \pm 0.2$ MJy sr$^{-1}$ ($10^{20}$ H atom cm$^{-2}$)$^{-1}$. Boulanger and Pérault (1988) derived average emissivity values for the entire high-latitude sky ($|b| > 10°$): $\varepsilon_{100,\,\mathrm{H\,I}} = 0.85 \pm 0.05$ and $\varepsilon_{60,\,\mathrm{H\,I}} = 0.18 \pm 0.01$ MJy sr$^{-1}$ ($10^{20}$ H atom cm$^{-2}$)$^{-1}$. These results are in agreement with our "local" values, simply defining these as the average of the emissivities in the 8–10 and 10–12 kpc rings: $\varepsilon_{100,\,\mathrm{H\,I}}(R_\odot) \simeq 0.8$ and $\varepsilon_{60,\,\mathrm{H\,I}}(R_\odot) \simeq 0.2$ MJy sr$^{-1}$ ($10^{20}$ H atom cm$^{-2}$)$^{-1}$. Clearly more detailed comparison is not warranted, because our local emissivity values are poorly defined, owing to the steep emissivity gradient. The average Galactic 60 μm/100 μm ratios of ~0.27 and ~0.20 which we found for dust mixed with atomic gas and molecular gas, respectively, are in the range of typical values at high latitudes. For comparison, Boulanger and Pérault (1988) derived an average value of $0.21 \pm 0.02$ at $|b| > 10°$.

For dust associated with molecular gas, our $Y_{100}$ estimate can be compared with the values obtained from several correlation studies of CO, H I, and 100-μm observations of individual clouds at high latitudes. A compilation is presented in Table 4; most authors do not give explicitly the $Y_{100}$ value, but it is readily derived from other quantities given. There is a remarkably small spread in the $Y_{100}$ estimates, which may have important implications for the $N_{\mathrm{H_2}}/W_{\mathrm{CO}}$ conversion factor $X$, to which we return in Sect. 4.3.

Our estimate of the isotropic background level at 100 μm ($I_{\mathrm{b},100} = 2.0 \pm 0.3$ MJy sr$^{-1}$) is in good agreement with the value of $1.8 \pm 0.3$ MJy sr$^{-1}$ derived by Boulanger and Pérault (1988) from an $I_{100} - N_{\mathrm{H\,I}}$ correlation study near the Galactic poles.

### 4.2. The radial FIR emissivity distribution and the contribution from small particles

The constancy of the 60 μm/100 μm emissivity ratio throughout the Galaxy (already noted by Burton et al., 1986), cannot easily be reconciled with current models for the heating of dust in the ISM. The strong radial gradient of the infrared emissivity distribution in the inner Galaxy (Fig. 4) together with the constancy of the 60 μm/100 μm emissivity ratio suggests, at first glance, a strong radial gradient in the dust-to-gas ratio. Between $R_\odot$ and $R = 5$ kpc, the emissivity increases by a factor of ~8. The energy density of the Galactic interstellar radiation field (ISRF), however, is generally estimated to increase by roughly the same factor (Mathis et al., 1983). The radial gradient in the ISRF should

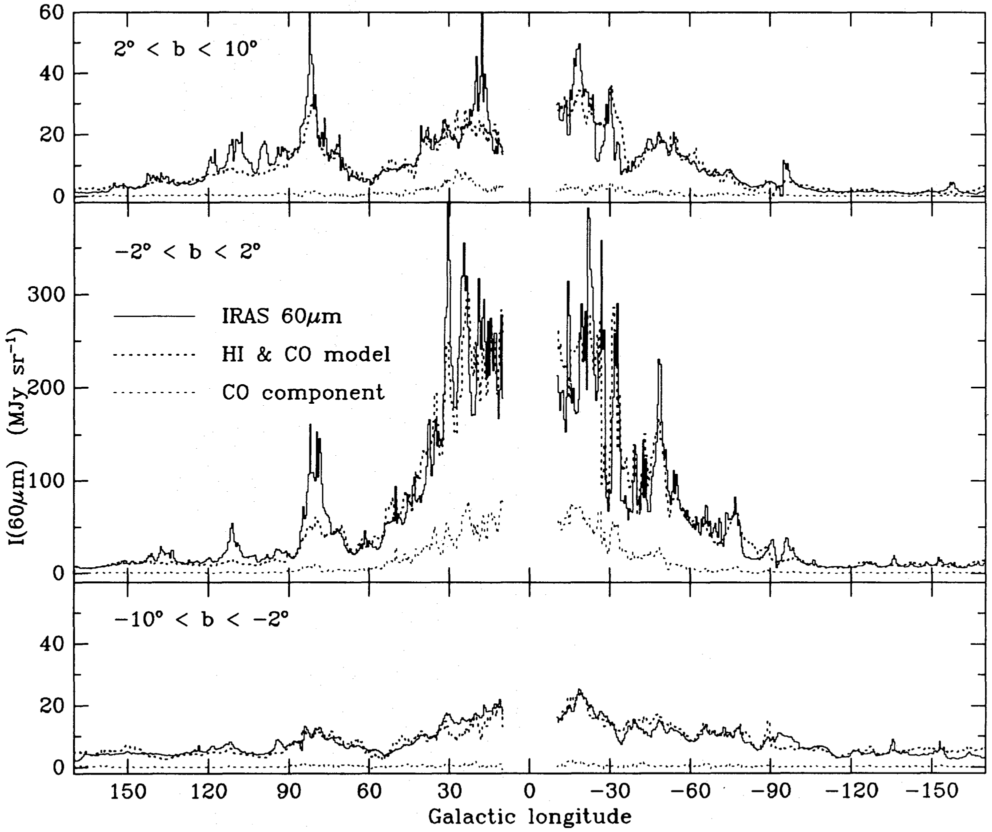


**Fig. 5.** Longitude distributions of the observed and expected infrared intensities in the 60-μm band as derived for case 2. The regions excluded from the analysis because of the presence of intense H II regions, poor kinematic-distance information, and striping artifacts are excluded from these profiles as well. The peaks in the observed profile, not fitted by the model, result from H II regions not rejected by the exclusion criterion (see Sect. 3.3)

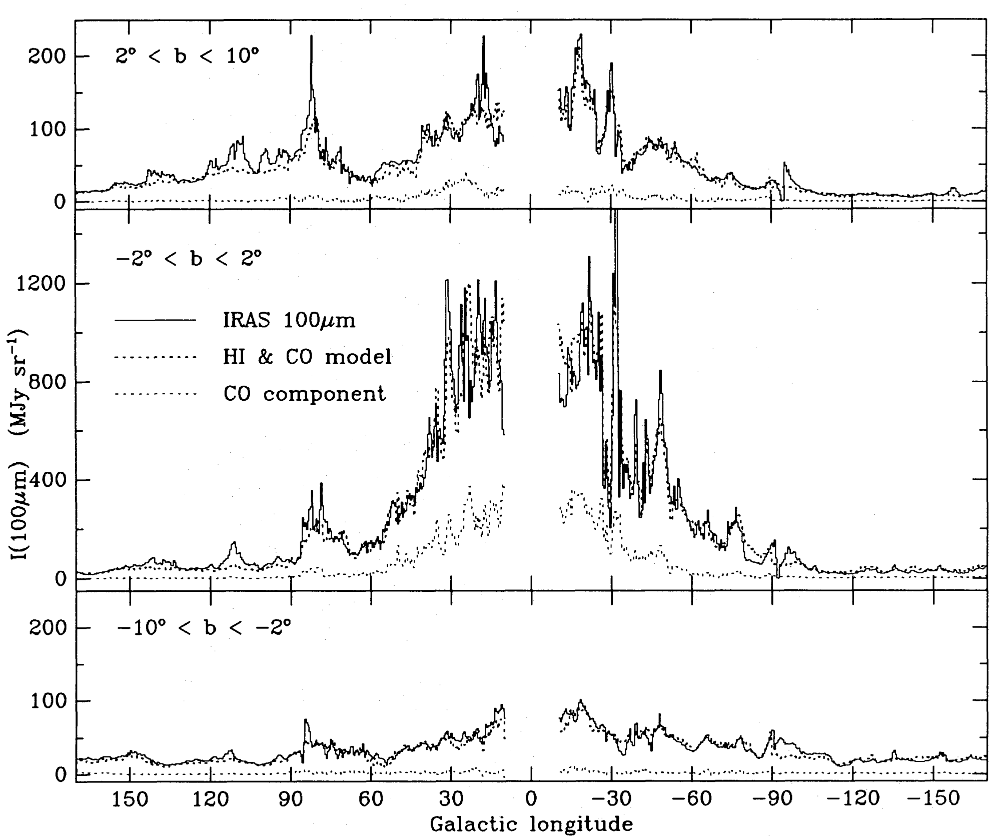


**Fig. 6.** The same as Fig. 5, except for the 100-μm band. The pronounced peaks in the observed profile at 60 μm, not fitted by the model, are less intense at 100 μm because the dust in the H II regions emits more strongly at 60 μm

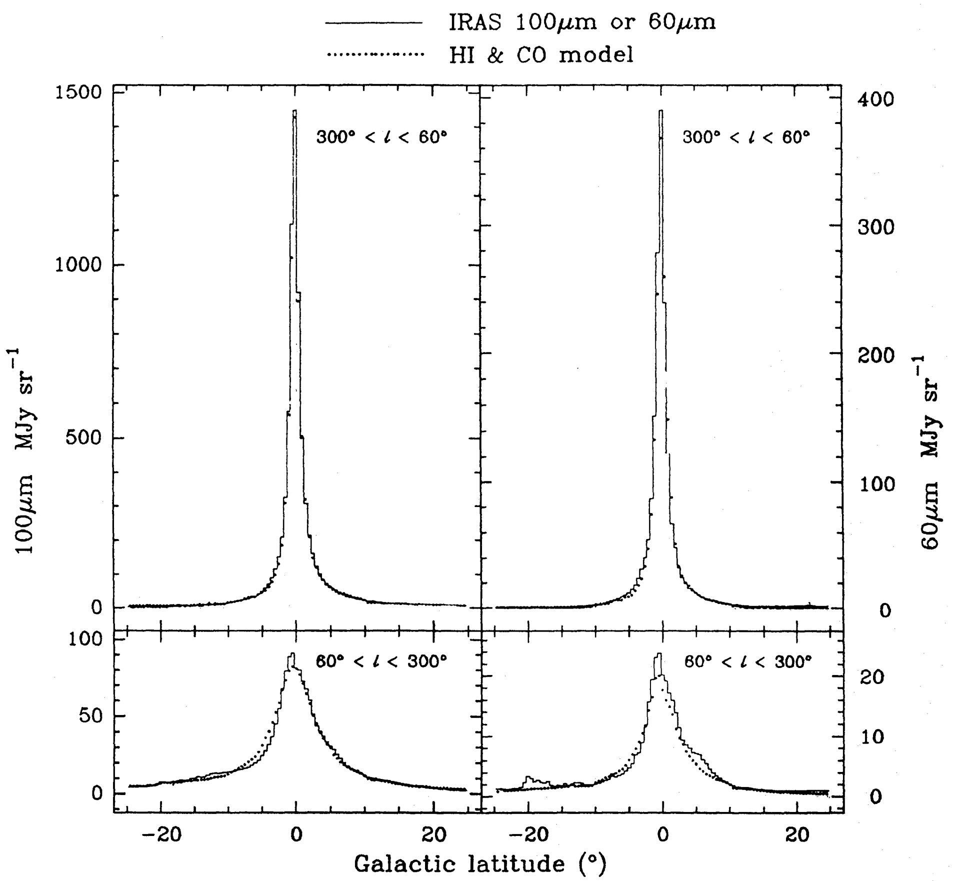


**Fig. 7.** Latitude distributions of the observed and expected infrared intensities in the 60-μm and 100-μm bands. The regions excluded from the analysis because of the presence of intense H II regions, poor kinematic-distance information, and striping artifacts are excluded from these profiles as well. The region fitted was restricted to $|b| < 10°$

**Table 4.** Values of $Y_{100}$, either given in the reference or derived from quantities therein. These can be regarded as estimates of the $N_{H_2}/W_{CO}$ ratio if the 100-μm emissivity (per nucleon) would be the same inside and outside the molecular cloud(s) (see Sect. 4.3)

| Reference | $Y_{100}$ [a] | Clouds |
|---|---|---|
| Weiland et al. (1986) | 0.6 [b] | HLC 16, 20, 30 of Magnani et al. (1985) |
| de Vries et al. (1987) | 0.5 | Ursa Major (Lynds 683) |
| de Geus (1988) | 0.6 | Ophiuchus |
| Heithausen and Mebold (1989) | 0.6 | Ursa Major (Lynds 629, 683, 691) |
| Boulanger [et al.] (1989) [c] | 0.4–0.6 | Auriga, Cepheus, Chamaeleon Lupus, Mon R2, Taurus |
| | 0.9 | Orion |
| Pérault et al. (1989) | 0.8 | Galactic disk |
| Sodroski et al. (1989) | 0.7 | Galactic disk |
| This work | 0.8 | Galactic disk |

[a] Units: $10^{20}$ molecules $cm^{-2}$ $(K\,km\,s^{-1})^{-1}$.
[b] From $I_{100}/W_{CO}$, assuming $\varepsilon_{100,HI} = 1$ MJy $sr^{-1}$ $(10^{20}$ H atom $cm^{-2})^{-1}$.
[c] Regions with clear evidence for star formation excluded, mainly important for Orion.

therefore be the preferred interpretation of the radial gradient in the infrared emissivity distribution we find, but the constancy of the 60 μm/100 μm emissivity ratio is difficult to understand in this case. For the standard grains of the model of Mathis, Rumpl, and Nordsieck (1977, hereafter MRN), with grain radii larger than 200 Å, such an increase in the intensity of the ISRF leads to an increase in the 60 μm/100 μm ratio from ~0.1 to 0.25 (e.g., Draine and Lee, 1984). An average Galactic value of ~0.27, such as we measured for the dust emission from atomic gas, is therefore problematic.

Draine and Anderson (1985) have shown that larger 60 μm/100 μm emissivity ratios are explained if the MRN power-law grain-size distribution extends to very small grain radii (a few Å), but the 60 μm/100 μm ratio will still increase significantly with increasing energy density of the general ISRF, and a value as high as 0.27 is reached only if the ISRF is several times more intense than measured in the solar vicinity (see their Fig. 4). They found, however, that values this high, with only a weak dependence on the ISRF, can be obtained if the abundances of the smallest particles are enhanced relative to the extended MRN size distribution. In this case, the relative unimportance of the ISRF is due to the weaker temperature dependence of the nonequilibrium emission from small grains relative to the equilibrium emission from large grains.

It can be concluded that in the framework of a grain model with an enhanced small particle distribution (or possibly large molecules; Léger and Puget 1984; Puget et al., 1985), the strong radial infrared emissivity gradient in the inner Galaxy may be largely explained by the increase of the energy density of the ISRF with decreasing Galactocentric radius. In view of the uncertainties both in the latter and in our estimate of the 60 µm/100 µm ratio, however, an increase in the dust-to-gas ratio by a factor of 2 between $R_\odot$ and $R = 5$ kpc probably cannot be excluded.

Figure 4 shows no evidence for a strong decrease of the emissivity beyond the solar circle to at least $R \simeq 17$ kpc (the approximate gas-mass-weighted radius of the outer ring in our analysis), although the average emissivity value of $\sim 0.4$ MJy sr$^{-1}$ ($10^{20}$ H atom cm$^{-2}$)$^{-1}$ (in the 100-µm band) is smaller than the value in the solar vicinity. This average value is consistent with the emissivities derived by Terebey and Fich (1986) for two selected outer Galaxy regions.

Within the uncertainties of our analysis, the radial dependence of the emissivity distribution for dust associated with molecular gas does not differ from that for dust mixed with atomic gas, but the 60 µm/100 µm emissivity ratio for the molecular component is smaller, namely $0.20 \pm 0.06$. Owing to the relatively large error, we cannot exclude the possibility that this ratio shows some variation with $R$. The low average 60 µm/100 µm emissivity ratio together with this possibility of radial dependence (i.e., an increase with increasing emissivity) may indicate that the contribution from small grains to the infrared emission from molecular clouds is less strong than that for atomic gas. This would not be surprising, because the heating of the small grains is to a large extent due to UV photons (Draine and Lee, 1984; Puget et al., 1985), from which the majority of the molecular gas traced by CO is shielded. The limb brightening at 12 µm of the Barnard 5 cloud found by Langer et al. (1989) may be direct evidence for such shielding.

Pérault et al. (1989) have derived the radial emissivity distribution in the inner Galaxy from a comparison of the observed 100-µm longitude profiles at $|b| = 0°, 1°, 2°$, and $3°$ with an empirical gas model derived from H I and CO observations [using $X = 2.5\ 10^{20}$ molecules cm$^{-2}$ (K km s$^{-1}$)$^{-1}$]. They separately studied the emissivity distributions of the dust components associated with atomic and molecular gas which were found to be very similar to the distributions we determined.

### 4.3. *FIR emission from molecular clouds and the $N_{H_2}/W_{CO}$ conversion factor*

In order to derive $X$ from our $Y_\lambda$ one needs to know the ratio between the infrared emissivities per nucleon inside and outside molecular clouds, that is, $\varepsilon_{\lambda, H_2}/\varepsilon_{\lambda, HI}$ (see Eq. 2). This ratio can be expected to vary among clouds of different categories (discussed below); we should focus on giant molecular clouds, which dominate the CO emission from the Galactic disk. In principle, both $Y_{60}$ and $Y_{100}$ can be used to derive $X$. They can be combined in an elegant way if the 60 µm/100 µm colour would be a good indicator of the dust temperature, but owing to the probably significant contribution from small grains to the emission in the 60-µm band this approach is not feasible. Further, this procedure would be sensitive to the contamination from H II regions not excluded by our criterion. Because both the presence of small particles and the remaining H II regions mainly affect the parameter estimates for the 60-µm band, the most reliable constraint on $X$ can be obtained from the 100-µm band alone, on which we concentrate in the following discussion.

The close resemblence between the observed 100-µm emission and our model (Fig. 6), with a simple axisymmetric dust emissivity distribution, suggests that mainly the general ISRF, rather than the radiation from embedded and nearby stars, is responsible for heating the dust in molecular clouds. Boulanger and Pérault (1988) demonstrated that indeed only high-mass stars, developing an H II region, are relevant local heating sources; only giant molecular clouds with masses larger than $10^5\,M_\odot$ have a high probability of forming such stars. Further, studies of nearby clouds associated with H II regions (Leisawitz and Hauser, 1988) show that only during the initial phase of its lifetime, an OB association heats its parent molecular cloud; stars in older subassociations, away from the cloud, can be considered contributors to the general ISRF. The regions most affected by high-mass star formation (H II regions and their interfaces with molecular clouds) are apparently mostly excluded by the criterion we applied. Approximately half of the total Galactic CO emission appears to originate from cool molecular clouds, not associated with (giant) H II regions (e.g., Stark, 1979; Solomon et al., 1985) and can therefore be expected to be heated predominantly by the general ISRF.

We proceed on the assumptions that the external ISRF is the dominant dust heating source for most of the molecular gas and that the dust properties and gas-to-dust ratio inside molecular clouds do not differ significantly from those in the ambient atomic medium. The average FIR emissivity from a cloud is then largely determined by its optical depth and geometry, since these determine the attenuation of the radiation field and therefore the average heating rate inside a cloud. For the simple case of a uniform, spherical cloud heated from outside by a uniform radiation field, Boulanger and Pérault (1988) derived explicit values of the ratio between the 100-µm emissivities inside and outside the cloud (in our notation, $\varepsilon_{100, H_2}/\varepsilon_{100, HI}$), from studies of radiative transfer and dust heating by Flannery et al. (1980) and Mathis et al. (1983). They found that for total visual extinctions, $A_v$, of 2, 5, and 10 mag through the centre of the cloud, $\varepsilon_{100, H_2}/\varepsilon_{100, HI} = 0.54$, 0.37, and 0.25, respectively. Although the actual geometry of a molecular cloud is undoubtedly important, their modelling indicates that the radiation field inside large clouds is attenuated on average by a factor of at least 2. This attenuation implies, according to our Eq. 2, that $Y_{100}$ is a strict lower limit on the average Galactic $X$ value [i.e., $X > 0.8\ 10^{20}$ molecules cm$^{-2}$ (K km s$^{-1}$)$^{-1}$] and, more likely, $X \gtrsim 2\,Y_{100}$, or $X \gtrsim 1.6\ 10^{20}$.

This lower limit on $X$ can be directly compared with the estimate obtained from an analysis of the COS-B $\gamma$-ray observations, using the same Columbia CO survey and fitting the same region of the sky (Strong et al., 1988). The best-fit value was found to be $(2.3 \pm 0.3)\ 10^{20}$ molecules cm$^{-2}$ (K km s$^{-1}$)$^{-1}$, although this value is arguably an upper limit to $N_{H_2}/W_{CO}$ owing to a possible contribution from $\gamma$-ray point sources and a possibly enhanced cosmic-ray density in molecular clouds. As in Section 3.3, the $\gamma$-ray analysis shows no significant difference between the average $X$ value (more precisely, $Y_\lambda$ value) for $R = 2$–$8$ kpc and that obtained for $R > 8$ kpc. The $\gamma$-ray estimate of $X$ is probably the most reliable one for large-scale studies, so contrary to the above approach, this $X$ may be used to determine the FIR emissivity inside molecular clouds relative to that in the surrounding medium, given by $Y_{100}/X$. The resulting value is $\sim 0.35$. In other words, if the $X$ estimate obtained by the COS-B group is adopted, then the 100-μm emissivity for the Galactic molecular cloud ensemble is on average $\sim 1/3$ that for the atomic gas located at approximately the same Galactocentric radius.

The consistency between our $Y_{100}$ value of $\sim 0.8\ 10^{20}$ and the values that follow from two other IRAS studies of the Galactic disk is gratifying. From the results presented by Pérault et al. (1989) we derive $Y_{100} \simeq 0.8\ 10^{20}$, and from Sodroski et al. (1989), $Y_{100} \simeq 0.7\ 10^{20}$. Both groups do not explicitely determine $Y_{100}$ (they use the $\gamma$-ray estimate of $X$), but the values follow directly from further quantities given. This consistency is of particular interest because widely different methods of analysis were used, especially in the treatment of H II regions, illustrating, once more, that the specific way of dealing with this phase of the ISM has no important impact on other parameter estimates. Another approach was followed by Broadbent et al. (1989), but we cannot easily check whether their findings agree as nicely.

We noted in Sect. 4.1 that our $Y_{100}$ estimate and the values obtained from correlation studies of CO, H I, and 100-μm observations of several local molecular clouds all are very similar, within a factor of about 2 (see Table 4). Considering the diverse types of clouds studied, this similarity is quite remarkable (although further substantiation is needed). The clouds span a considerable range in optical depths, so, as discussed above, $\varepsilon_{100,\mathrm{H_2}}/\varepsilon_{100,\mathrm{H\,I}}$, and thus $Y_{100}$, is expected to vary. Note that the trend visible in Table 4 (larger $Y_{100}$ values for giant molecular clouds) is quite opposite to this expectation, even if a substantial fraction of the CO and FIR emission originates from relatively diffuse parts. The small spread in $Y_{100}$ values suggests, therefore, that different $X$ values apply to different categories of molecular clouds. More precisely, for clouds predominantly heated by the ambient ISRF, $X$ appears to be anticorrelated with the average FIR emissivity per nucleon inside the clouds relative to that in the surrounding medium and thus correlated with the total extinction of the clouds (for $A_v > 1$ mag). The underlying reason may be the inverse proportionality between $X$ and the gas temperature, predicted by models (Kutner and Leung, 1985; van Dishoeck and Black, 1987; Maloney and Black, 1988). For $A_v < 1$ mag, $X$ should be approximately equal to $Y_{100}$ according to these models, but the CO emission from such diffuse, and mostly young, clouds (e.g., the so called high-latitude clouds; Magnani et al., 1985), can be expected to be influenced by various other effects (see Magnani et al., 1988).

### 4.4. FIR luminosities

We can use our $\varepsilon_\lambda$ and $Y_\lambda$ values together with additional information on the radial distribution of the gas to determine the FIR luminosities for selected Galactocentric rings at $R > 2$ kpc, defined as

$$L_{\mathrm{FIR,H\,I}} = M_{\mathrm{H\,I}} \sum_{\lambda = 60, 100\,\mu\mathrm{m}} 4\pi\lambda\varepsilon_\lambda \tag{8a}$$

and

$$L_{\mathrm{FIR,H_2}} = M_{\mathrm{H_2}} \sum_{\lambda = 60, 100\,\mu\mathrm{m}} 4\pi\lambda\varepsilon_\lambda \frac{Y_\lambda}{X}. \tag{8b}$$

The results are summarized in Table 5. We obtained the $H_2$ mass in each ring at $R < R_\odot$ from the radial distribution of the $H_2$ surface density derived by Bronfman et al. (1988) from the Columbia CO survey. For $R > R_\odot$, the $H_2$ mass derived by Bloemen et al. (1986) from the Columbia data was used. Details regarding the dependence on $X$ are given in the footnotes of

**Table 5.** Gas masses, FIR emissivities, and luminosities (sum of the emission in the 60-μm and 100-μm bands)

| $R$ (kpc) | $M_{\mathrm{H_2}}$ [a] ($M_\odot$) | $\frac{L_{\mathrm{FIR,H_2}}}{M_{\mathrm{H_2}}}$ [b,c] ($L_\odot/M_\odot$) | $L_{\mathrm{FIR,H_2}}$ ($L_\odot$) | $M_{\mathrm{H\,I}}$ [f,h] ($M_\odot$) | $\frac{L_{\mathrm{FIR,H\,I}}}{M_{\mathrm{H\,I}}}$ [b] ($L_\odot/M_\odot$) | $L_{\mathrm{FIR,H\,I}}$ [h] ($L_\odot$) |
|---|---|---|---|---|---|---|
| 2–4 | $6.8\ 10^7$ [d] | 11.3 | $7.7\ 10^8$ | $6.0\ 10^7$ | 33.3 | $2.0\ 10^9$ |
| 4–8 | $7.2\ 10^8$ [d] | 2.2 | $1.6\ 10^9$ | $4.4\ 10^8$ | 6.6 | $2.9\ 10^9$ |
| 8–10 | $2.2\ 10^8$ [d] | 0.74 | $1.6\ 10^8$ | $3.3\ 10^8$ | 2.1 | $6.9\ 10^8$ |
| 10–15 | $1.9\ 10^8$ [e] | 0.23 | $4.4\ 10^7$ | $1.1\ 10^9$ | 0.69 | $7.6\ 10^8$ |
| >15 | – | – | – | $2.8\ 10^9$ [g] | 0.47 | $1.3\ 10^9$ |
| 2–10 | $1.0\ 10^9$ | | $2.5\ 10^9$ | $8.3\ 10^8$ | | $5.6\ 10^9$ |
| >10 | $1.9\ 10^8$ | | $4.4\ 10^7$ | $3.9\ 10^9$ | | $2.1\ 10^9$ |
| total | $1.2\ 10^9$ | | $2.5\ 10^9$ | $4.8\ 10^9$ | | $7.7\ 10^9$ |

[a] Values can be scaled by $X/2.3\ 10^{20}$.
[b] Table 3, case 2.
[c] Values can be scaled by $2.3\ 10^{20}/X$.
[d] Bronfman et al. (1988), scaled to $X = 2.3\ 10^{20}$ molecules cm$^{-2}$ (K km s$^{-1}$)$^{-1}$.
[e] Bloemen et al. (1986), scaled to $X = 2.3\ 10^{20}$ molecules cm$^{-2}$ (K km s$^{-1}$)$^{-1}$.
[f] Based on Henderson et al. (1982), with a constant value of $\sigma_{\mathrm{H\,I}} = 2.9\ M_\odot\ \mathrm{pc}^{-2}$ for $R = 4$–15 kpc and half that value for $R = 2$–4 kpc.
[g] From estimate of total H I mass in the Galaxy obtained by Henderson et al. ($4.8\ 10^9\ M_\odot$), minus H I mass for $R < 15$ kpc.
[h] See Sect. 4.4 for discussion on high-$z$ H I.

Table 5. Note that $M_{H_2}$ scales with $X$, so $L_{FIR, H_2}$ does not depend on $X$. The H I masses given in the table are based on mass estimates obtained by Henderson et al. (1982). The H I surface density was assumed to be constant from $R = 4$ kpc to 15 kpc, as shown by Gordon and Burton (1976) and Blitz et al. (1983), and its value ($\sigma_{HI} = 2.9\,M_\odot\,pc^{-2}$) was derived from the total H I mass at $R < 10$ kpc of 0.9 $10^9\,M_\odot$ found by Henderson et al. (1982). For $R = 2$–4 kpc, $\sigma_{HI}$ is uncertain; we used 1.5 $M_\odot\,pc^{-2}$. The H I mass at $R > 15$ kpc follows then from the total H I mass in the Galaxy of 4.8 $10^8\,M_\odot$ found by Henderson et al.

We see from Table 5 that the total luminosity of the FIR emission (60-μm and 100-μm bands) which we have attributed to dust mixed with atomic and molecular gas in the Galactic disk is about 1.0 $10^{10}\,L_\odot$ ($R > 2$ kpc), of which $\sim 3/4$ originates from dust associated with H I. About 3/4 of the emission originates inside the solar circle ($R = 2$–10 kpc). Studies by Lockman (1984) and Lockman et al. (1986) have revealed high-$z$ H I at $R \lesssim R_\odot$ not recognized in previous 21-cm studies. This gas, with a scale height of $\sim 400$ pc and a surface density as large as $\sim 2\,M_\odot\,pc^{-2}$, may not be included in the H I mass estimates derived by Henderson et al. (1982), which we used. If so, and on the assumption that this broad H I component extends to $R \simeq 15$ kpc, it may account for an additional FIR luminosity of $\sim 3\,10^9\,L_\odot$, of which about 2/3 originates inside the solar circle.

The FIR luminosity of warm dust associated with ionized gas cannot be accurately estimated, but appears to be small. We have already noted the generally good agreement between the observed infrared emission and the modelled emission based on H I and CO data alone, except for some strong peaks in the infrared data. The integrated flux of these excesses, not explained by our model, as well as the flux of the infrared peaks in the regions excluded from our analysis (with $I_{60\,\mu m}/I_{100\,\mu m} > 0.35$) comprise only a small fraction of the total flux from the Milky Way. This indicates that the FIR luminosity of any component not included in our model contributes only a small fraction to the total Galactic luminosity. On the other hand, the infrared emission we relate to molecular clouds may actually partly originate from warm dust in star-forming regions near the clouds, although the relatively low 60 μm/100 μm ratio of $\sim 0.2$ we found for this component makes this fraction seem rather small.

Other recent large-scale studies of the IRAS observations of the Galactic disk have led to similar estimates of the FIR luminosity related to H I gas and its relative contribution ($\sim 3/4$) to the total Galactic emission (Cox and Mezger, 1988, 1989; Pérault et al., 1989; Sodroski et al., 1989; Pérault et al.). There is no real consensus, however, on the origin of the remaining 1/4. Pérault et al. (1989), Sodroski et al. (1989), and we ourselves tend to attribute it largely to relatively cool dust associated with $H_2$ gas, while Cox and Mezger (1988; 1989) prefer an origin largely in OB star-forming regions and extended low-density H II regions.

### *4.5. Comparison with M 31*

Walterbos and Schwering (1987) have studied IRAS observations of the Andromeda galaxy and reached conclusions very similar to ours. A comparison with H I observations showed an essentially monotonic decrease of the 60-μm and 100-μm emissivities with galactic radius, as we found, with the same remarkable constancy of the 60 μm/100 μm emissivity ratio ($\sim 0.2$, so somewhat lower than the value in our Galaxy). They concluded from the relatively low temperature (21–22 K) and the structure of the emission that most of the FIR emission results from dust associated with atomic gas heated by the general ISRF. As we conclude for our Galaxy, they found that the luminosity of warm dust ($\sim 40$ K) associated with star-formation regions is only a small fraction (< 10%) of the total infrared luminosity, about 2.6 $10^9\,L_\odot$. Their discussion of the relatively low contribution from warm dust in M 31 compared with our Galaxy [on the basis of the high estimates from Mezger et al. (1982) and Cox et al. (1986)] therefore no longer appears applicable; we noted above that recent estimates by Cox and Mezger (1988; 1989) are much lower and not drastically different from our findings.

## 5. Conclusions

Our main conclusions can be summarized as follows:

1. The FIR emission of the Milky Way in the 60-μm and 100-μm IRAS bands at $R > 2$ kpc originates largely from dust associated with neutral atomic gas ($\sim 8$–11 $10^9\,L_\odot$) and molecular gas ($\sim 2.5\,10^9\,L_\odot$) heated by the general ISRF. Infrared emission from dust associated with H II regions appears to contribute only a minor fraction to the Galactic FIR luminosity. Most ($\sim 3/4$) of the Galactic FIR emission originates inside the solar circle: $\sim 6$–8 $10^9\,L_\odot$ from dust associated with H I and $\sim 2.5\,10^9\,L_\odot$ from dust associated with molecular gas (both for $R = 2$–10 kpc).

2. The infrared dust emissivity per nucleon decreases strongly between $R \simeq 5$ kpc and $R_\odot$ (by a factor of $\sim 8$). Beyond the solar circle, the decrease is not so precipitous. There is no indication that the emissivity distribution peaks near the molecular ring at $R \simeq 5$ kpc or that it flattens for $R < 5$ kpc, although it is not well determined at small Galactic radii. The shape of the radial distribution is similar for both passbands and also similar for dust mixed with atomic and molecular gas. The average Galactic 60 μm/100 μm emissivity ratios are $0.27 \pm 0.03$ and $0.20 \pm 0.06$ for dust mixed with atomic and molecular gas, respectively. The emissivity per nucleon for dust in molecular clouds (excluding the interfaces with H II regions) is on average about 1/3 that for dust in the atomic gas, if the $N_{H_2}/W_{CO}$ calibration factor obtained from $\gamma$-ray studies is adopted (see 4 below).

3. A significant contribution from small grains to the 60-μm emission of dust associated with the atomic component is suggested by the similarity of the emissivity gradients at 60 μm and 100 μm with a 60 μm/100 μm ratio as high as $\sim 0.27$. This similarity can be understood in terms of the grain model of Draine and Anderson (1985), with the abundances of the smallest particles enhanced relative to the Mathis-Rumple-Nordsieck power-law size distribution. The contribution from these small grains to the infrared emission from molecular clouds may be less than for the atomic gas. The radial emissivity gradient can be attributed entirely to the variation of the intensity of the ISRF, but an increase in the dust-to-gas ratio by a factor of 2 between $R_\odot$ and $R = 5$ kpc probably cannot be excluded.

4. A strict lower limit on the average Galactic value of the ratio between $H_2$ column density and integrated CO-line intensity was obtained from the 100-μm emission: $X \gtrsim 0.8\,10^{20}$ molecules $cm^{-2}\,(K\,km\,s^{-1})^{-1}$. To find the true $X$ value, this lower limit should be divided by the ratio of the average 100-μm emissivity inside molecular clouds to the average in the ambient atomic gas. Modelling has shown that this ratio probably does not exceed a value of about 0.5 for the clouds that dominate the CO emission from the Galactic disk, implying that $X \gtrsim 1.6\,10^{20}$ for the Galactic cloud ensemble. For the independent COS-B $\gamma$-ray estimate of $X$ ($\sim 2.3\,10^{20}$) the molecular-to-atomic dust emissivity ratio is about 1/3.

An intercomparison of our study of molecular clouds in the Galactic disk and other FIR studies of individual molecular clouds at high latitudes indicates that, for clouds predominantly heated by the external ISRF, $X$ is anticorrelated with the FIR (100-μm) emissivity per nucleon inside the cloud relative to that in the surrounding medium. This suggests a correlation between $X$ and the total extinction of clouds with $A_v > 1$ mag, in accordance with expectations. Further substantiation is needed.

*Acknowledgements.* We thank F. Boulanger, P. Cox, M. Pérault, and R. A. M. Walterbos for useful comments. H. B. acknowledges the receipt of a Fellowship from the Royal Netherlands Academy of Arts and Sciences (KNAW).

**References**

Beichman, C.A.: 1987, *Ann. Rev. Astron. Astrophys.* **25**, 521
Blitz, L., Fich, M., Kulkarni, S.R.: 1983, *Science* **220**, 1233
Blitz, L., Fich, M., Stark, A.A.: 1980, in *Interstellar Molecules*, ed. B. Andrew, Reidel, Dordrecht, p. 213
Bloemen, J.B.G.M., Strong, A.W., Blitz, L., Cohen, R.S., Dame, T.M., Grabelsky, D.A., Hermsen, W., Lebrun, F., Mayer-Hasselwander, H.A., Thaddeus, P.: 1986, *Astron. Astrophys.* **154**, 25
Boissé, P., Gispert, R., Coron, N., Wijnbergen, J.J., Serra, G., Ryter, C., Puget, J.L.: 1981, *Astron. Astrophys.* **94**, 265
Boulanger, F.: 1989, in *Physics and Chemistry of Interstellar Molecular Clouds*, eds. G. Winnewisser and J.T. Armstrong, Springer, Berlin, Heidelberg, New York, p. 30
Boulanger, F., Baud, B., van Albada, G.D.: 1985, *Astron. Astrophys. (Letters)* **144**, L9
Boulanger, F., Cohen, R.S., Gaida, M., Grenier, I., Koprucu, M., Maddalena, R.J., Thaddeus, P., Ungerechts, H.: 1989 (preprint)
Boulanger, F., Pérault, M.: 1988, *Astrophys. J.* **330**, 964
Broadbent, A., MacLaren, I., Wolfendale, A.W.: 1989, *Monthly Notices Royal Astron. Soc.* **237**, 1075
Bronfman, L., Cohen, R.S., Alvarez, H., May, J., Thaddeus, P.: 1988, *Astrophys. J.* **324**, 248
Burton, W.B., Deul, E.R., Walker, H.J., Jongeneelen, A.A.W.: 1986, in *Light on dark matter*, ed. F.P. Israel, Reidel, Dordrecht, p. 357
Burton, W.B., Gordon, M.A.: 1978, *Astron. Astrophys.* **63**, 7
Caux, E., Serra, G., Gispert, R., Puget, J.L., Ryter, C., Coron, N.: 1984, *Astron. Astrophys.* **137**, 1
Cox, P., Krügel, E., Mezger, P.G.: 1986, *Astron. Astrophys.* **155**, 380
Cox, P., Mezger, P.G.: 1988, in *Comets to Cosmology*, ed. A. Lawrence, Springer, Berlin, Heidelberg, New York, p. 97
Cox, P., Mezger, P.G.: 1989, *Astron. Astrophys. Review* **1**, 49
Dame, T.M., Ungerechts, H., Cohen, R.S., de Geus, E., Grenier, I., May, J., Murphy, D.C., Nyman, L.-Å., Thaddeus, P.: 1987, *Astrophys. J.* **322**, 706
Deul, E.R., Burton, W.B.: 1989, *Astron. Astrophys.* (submitted)
Deul, E.R., Wolstencroft, R.W.: 1988, *Astron. Astrophys.* **196**, 277
van Dishoeck, E.F., Black, J.H.: 1987, in *Physical Processes in Interstellar Clouds*, eds. G.E. Morfill and M. Scholer, Reidel, Dordrecht, p. 241
Draine, B.T., Anderson, N.: 1985, *Astrophys. J.* **292**, 494
Draine, B.T., Lee, H.M.: 1984, *Astrophys. J.* **285**, 89
Drapatz, S.: 1979, *Astron. Astrophys.* **75**, 26
Eadie, W.T., Drijard, D., James, F.E., Roos, M., Sadoulet, B.: 1971, in *Statistical Methods in Experimental Physics*, North Holland, Amsterdam, p. 230
Flannery, B.P., Roberge, W., Rybicki, G.B.: 1980, *Astrophys. J.* **236**, 598
de Geus, E.J.: 1988, PhD Thesis, University of Leiden
Gispert, R., Puget, J.L., Serra, G.: 1982, *Astron. Astrophys.* **106**, 293
Gordon, M.A., Burton, W.B.: 1976, *Astrophys. J.* **208**, 346
Hauser, M.G., Silverberg, R.F., Stier, M.T., Kelsall, T., Gezari, D.Y., Dwek, E., Walser, D., Mather, J.C., Cheung, L.H.: 1984, *Astrophys. J.* **285**, 74
Heiles, C., Habing, H.J.: 1974, *Astron. Astrophys. Suppl.* **14**, 1
Heiles, C., Cleary, M.N.: 1979, *Australian J. Phys. Suppl.* **47**, 1
Heithausen, A., Mebold, U.: 1988, *Astron. Astrophys.* **214**, 347
Henderson, A.P., Jackson, P.D., Kerr, F.J.: 1982, *Astrophys. J.* **263**, 182
IRAS Explanatory Supplement: 1985, Beichman, C.A., Neugebauer, G., Habing, H.J., Clegg, P.E., Chester, T.J. (eds.), Jet Propulsion Laboratories, Gainsville
Kendall, M.G., Stuart, A.: 1973, *The Advanced Theory of Statistics*, Vol. II, Griffin, London
Kerr, F.J., Bowers, P.F., Jackson, P.D., Kerr, M.: 1986, *Astron. Astrophys. Suppl.* **66**, 373
Kulkarni, S.R., Blitz, L., Heiles, C.: 1982, *Astrophys. J. Lett.* **259**, L63
Kutner, M.L., Leung, C.M.: 1985, *Astrophys. J.* **291**, 188
Langer, W.D., Wilson, R.W., Goldsmith, P.F., Beichman, C.A.: 1989, *Astrophys. J.* **337**, 355
Léger, A., Puget, J.L.: 1984, *Astron. Astrophys. (Letters)* **137**, L5
Leisawitz, D., Hauser, M.: 1988, *Astrophys. J.* **332**, 954
Lockman, F.J.: 1984, *Astrophys. J.* **283**, 90
Lockman, F.J., Hobbs, L.M., Shull, J.M.: 1986, *Astrophys. J.* **301**, 380
Low, J.J., Beintema, D.A., Gautier, T.N., Gillet, F.C., Beichman, C.A., Neugebauer, G., Young, E., Aumann, H.H., Boggers, N., Emerson, J.P., Habing, H.J., Hauser, M.G., Houck, J.R., Rowan-Robinson, M., Soifer, B.T., Walker, R.G., Wesselius, P.R.: 1984, *Astrophys. J. Lett.* **278**, L19
Magnani, L., Blitz, L., Mundy, L.: 1985, *Astrophys. J.* **295**, 402
Magnani, L., Blitz, L., Wouterloot, J.G.A.: 1988, *Astrophys. J.* **326**, 909
Maloney, P., Black, J.H.: 1988, *Astrophys. J.* **325**, 389
Mathis, J.S., Mezger, P.G., Panagia, N.: 1983, *Astron. Astrophys.* **128**, 212
Mathis, J.S., Rumpl, W., Nordsieck, K.H.: 1977, *Astrophys. J.* **217**, 425
Mezger, P.G.: 1978, *Astron. Astrophys.* **70**, 565
Mezger, P.G., Mathis, J.S., Panagia, N.: 1982, *Astron. Astrophys.* **105**, 372
Nishimura, T., Low, F.J., Kurtz, R.F.: 1980, *Astrophys. J. Lett.* **239**, L101
Pérault, M., Boulanger, F., Puget, J.L., Falgarone, E.: 1989, *Astrophys. J.* (submitted)
Puget, J.L.: 1985, in *Les Houches Summerschool on Birth and Infancy of Stars*, eds. R. Lucas, A. Omont, R. Stora, Elsevier, Amsterdam, p. 77
Puget, J.L., Léger, A., Boulanger, F.: 1985, *Astron. Astrophys. (Letters)* **142**, L19
Ryter, C.E., Puget, J.L.: 1977, *Astrophys. J.* **215**, 775
Sodroski, T.J., Dwek, E., Hauser, M.G., Kerr, F.J.: 1989, *Astrophys. J.* **336**, 762

Solomon, P.M., Sanders, D.B., Rivolo, R.: 1985, *Astrophys. J. Lett.* **292**, L19
Stark, A.A.: 1979, Ph.D. Thesis, University of Princeton
Strong, A.W., Riley, P.A., Osborne, J.L., Murray, J.D.: 1982, *Monthly Notices Roy. Astron. Soc.* **201**, 495
Strong, A.W., Bloemen, J.B.G.M., Dame, T.M., Grenier, I.A., Hermsen, W., Lebrun, F., Nyman, L.A., Pollock, A., Thaddeus, P.: 1988, *Astron. Astrophys.* **207**, 1
Terebey, S., Fich, M.: 1986, *Astrophys. J. Lett.* **309**, L73
de Vries, H.W., Heithausen, A., Thaddeus, P.: 1987, *Astrophys. J.* **319**, 723
Walterbos, R.A.M., Schwering, P.B.W.: 1987, *Astron. Astrophys.* **180**, 27
Weaver, H., Williams, D.R.W.: 1973, *Astron. Astrophys. Suppl.* **8**, 1
Weiland, J.L., Blitz, L., Dwek, E., Hauser, M.G., Magnani, L., Rickard, L.J.: 1986, *Astrophys. J. Lett.* **306**, L101
Williams, D.R.W.: 1973, *Astron. Astrophys. Suppl.* **8**, 505